Analytical Methods

ROYAL SOCIETY OF CHEMISTRY

MINIREVIEW

Cite this: *Anal. Methods*, 2021, **13**, 1084

Recent advances in selective formaldehyde detection in biological and environmental samples by fluorometric and colorimetric chemodosimeters

Saikat Kumar Manna, *[a] Tapas Kumar Achar[b] and Sanchita Mondal [c]

Formaldehyde, a highly reactive carbonyl species, has been widely used in day-to-day life owing to its numerous applications in essential commodities, *etc.*; the extrusion of formaldehyde from these sources basically leads to increased formaldehyde levels in the environment. Additionally, formaldehyde is endogenously produced in the human body *via* several biological processes. Considering the adverse effects of formaldehyde, it is highly important to develop an efficient and reliable method for monitoring formaldehyde in environmental and biological samples. Several chemodosimeters (reaction-based sensing probes) have been designed and synthesized to selectively detect the presence of formaldehyde utilizing the photophysical properties of molecules. In this review, we have comprehensively discussed the recent advances in the design principles and sensing mechanisms of developed probes and their biological/environmental applications in selective formaldehyde detection and imaging endogenous formaldehyde in cells. We have summarized the literature based on three different categories: (i) the Schiff base reaction, (ii) the 2-aza-Cope sigmatropic rearrangement reaction and (iii) miscellaneous approaches. In all cases, reactions are accompanied by changes in color and/or emission that can be detected by the naked eye.

Received 9th December 2020
Accepted 1st February 2021

DOI: 10.1039/d0ay02252g

rsc.li/methods

1. Introduction

Formaldehyde (HCHO), a highly reactive colorless gas with a strong and pungent smell, has attracted tremendous attention from researchers due to its widespread application in many areas, such as plastics, cosmetics, food, drugs, wood processing (particleboard, oriented-strand board (OSB), high-density fiber board (HDF), furniture, medium density fiber board (MDF), and

[a]*Department of Chemistry, Haldia Government College, Debhog, Purba Medinipur, West Bengal-721657, India. E-mail: saikat.manna.chem@gmail.com*

[b]*Department of Chemistry, Indian Institute of Technology Bombay, Powai, Mumbai 400076, India*

[c]*Department of Chemistry, Jadavpur University, Kolkata 700032, India*

Dr Saikat Kumar Manna received his Ph.D. degree in organic chemistry from the Indian Institute of Engineering Science and Technology, Shibpur, Howrah, in 2015. He is currently working as an Assistant Professor in the Postgraduate Department of Chemistry, Haldia Government College, West Bengal, India. To date, he has authored 34 research publications. His research interests include molecular recognition and synthetic organic chemistry.

Tapas Kumar Achar received his Ph.D. from the National Institute of Science Education and Research (NISER), Bhubaneswar, in 2016 under the supervision of Prof. Prasenjit Mal. Then, he joined Prof. Debabrata Maiti's group at IIT Bombay as a SERB National Post-Doctoral Fellow in 2017. After finishing his postdoctoral stay at IIT Bombay, he joined the ORSY division at the University of Antwerp, Belgium, in 2019 as a postdoctoral research associate. His research interests mainly focus on transition metal-catalyzed remote C–H bond functionalization and asymmetric catalysis.

plywood), medical science, biotechnology, paints and textiles.[1–14] It is also employed as a cleaning and caring product, photoprocessing chemical, preservative, disinfectant, and biocide.[15] The aqueous solution of formaldehyde, called formalin, is used as a disinfectant in hospitals due to its antiseptic properties.[16] However, formaldehyde is considered to be the third largest indoor chemical pollutant, and it poses an important threat to living organisms because of its carcinogenic and mutagenic nature.[17–24] Generally, formaldehyde is released into the atmosphere from both natural (microbe emission, vegetation, degradation of humic substances, biomass combustion, *etc.*) and anthropogenic or artificial (vehicle exhaust, building ingredients, fumigation, industrial production of formaldehyde, *etc.*) sources.[25–27] Additionally, formaldehyde is endogenously generated in the human body during demethylation or oxidation processes catalyzed by demethylase and oxidase enzymes such as lysine-specific demethylase 1 (LSD1),[28–30] alcohol dehydrogenase (ADH), semicarbazide-sensitive amine oxidase (SSAO)[31] and JmjC domain-containing protein.[32–35] The normal level of formaldehyde in human blood is about 50–100 μM; that in cells is 200–400 μM, and that in the brain is 0.2–0.4 mM.[36–38] Regular formaldehyde concentration is associated with spatial memory and cognitive abilities;[39–41] however, the excess accumulation of formaldehyde in living organisms can trigger different diseases, such as Alzheimer's disease, inhibition of DNA repair, asthma, heart disorders, cancer, cirrhosis, leukemia, diabetes, neurological and cardiovascular disorders, chronic liver disorders, neonatal chromosome disorder, allergic pneumonia, impaired memory, and mutations of nuclear genes.[42–54] The World Health Organization (WHO) and the United States Environmental Protection Agency (US EPA) recommend a tolerable daily consumption of formaldehyde at 0.15 and 0.2 mg kg^{-1} body weight, respectively.[55–57]

Considering the adverse effects of formaldehyde, the development of convenient, proficient and reliable methods for monitoring formaldehyde in environmental and biological samples is highly desirable. Unstinting effort from the research community has aided the development of numerous analytical techniques for formaldehyde detection, such as high-performance liquid chromatography,[58] cataluminescence,[59] gas chromatography,[60] chemoresistivity,[61] organic–inorganic hybrid materials,[62] biosensor methods,[63] capillary electrophoresis,[64] field effect gas sensors,[65] ion chromatography,[66] polarography,[67] Raman spectroscopy,[68] sol–gel methods,[69] quartz crystal microbalance,[70] conductometry,[71] X-ray diffraction (XRD) and transmission electron microscopy (TEM).[72]

Recently, chromogenic and fluorogenic chemodosimeters for formaldehyde sensing have been developed as alternatives to these costly and time-consuming conventional processes.[73–77] The main reasons for the wide applicability of these spectral methods include their simplicity, selectivity, high sensitivity, rapidity, reliability, ease of application, economical nature and real-time monitoring in living cells and tissues.[78–80] Chemodosimeters are chemical systems that detect target analytes by means of a highly selective, sensitive and typically irreversible chemical reaction.[81,82] Here, all discussed chemodosimeters are designed so that changes in fluorescence and/or absorption are observed sharply upon reaction with the analyte, *i.e.*, formaldehyde.

The developments of this chemistry have been summarized in a few articles in a scattered way. However, in-depth mechanistic understanding can be realized by an inclusive survey of the research developments in chromogenic/fluorogenic chemodosimeters for selective detection of formaldehyde. The aim of this review is to provide a comprehensive understanding of this chemistry, encompassing the in-depth and exhaustive discussion of mechanistic considerations and covering recent developments from 2018 onwards along with unprecedented notable developments. In this review, we have discussed recent developments categorically in terms of mechanistic understanding: (i) the Schiff base reaction; (ii) the 2-aza-Cope sigmatropic rearrangement reaction; and (iii) miscellaneous approaches.

2. Formaldehyde-sensing mechanisms

2.1. Schiff base reaction

The hydrazine moiety or amine group is generally used as a selective reactive unit in the design and development of probes to sense formaldehyde. Formaldehyde reacts with hydrazine moiety/amine groups to form the corresponding imines (Schiff base reaction),[83–85] which show considerably different emission and absorption properties (Scheme 1). Based on this general strategy, in this section, we discuss various amine and hydrazine derivatives based on 1,8-napthalimides, benzooxazole, benzothiazole, tri-aryl pyridine, BODIPY, NBD

Dr Sanchita Mondal received her Ph.D. degree in 2017 from the Indian Institute of Engineering Science and Technology, Shibpur, Howrah. She is currently working as a Dr D. S. Kothari Postdoctoral Fellow in the Department of Chemistry, Jadavpur University. She has published more than 20 research papers in peer-reviewed international journals in the area of molecular recognition and supramolecular chemistry.

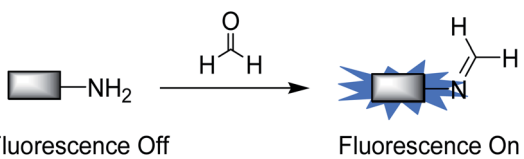

Scheme 1 Strategy for the design of formaldehyde-selective fluorescent probes based on the Schiff base reaction.

(nitrobenzoxadiazole) derivatives, metal–organic frameworks (MOF), chitosan-based polymers, rhodamine B, naphthalene, tetraphenyl ethylene (TPE) and perylene bisimide (PDI) to showcase fluorogenic and chromogenic chemodosimeters for the selective detection of formaldehyde.

2.1.1. Amine moiety-based chemodosimeters. A condensation reaction of aldehyde (formaldehyde) and amine functionalities provides the simplest Schiff base, formimine (Scheme 1), which can be utilized as an efficient technique for detection of formaldehyde analyte. Based on this principle, chemists have designed and developed numerous fluorescent probes for formaldehyde detection.

In 2012, Song *et al.*[86] first reported a Schiff base-based strategy for the selective detection of formaldehyde, which further inspired the development of several probes discussed in this review. Initially, probe **1** displayed weak fluorescence at 535 nm due to an effective PET quenching effect from the aniline group to the BODIPY moiety. However, the emission intensity at 535 nm increased gradually with the incremental addition of formaldehyde owing to the formation of an imine compound (**1a**), which eliminated the PET process. The detection limit of **1** for formaldehyde based on its fluorescence response is 165 nM, showing the highly sensitive efficiency of the chemosensor (Fig. 1).

Utilizing this approach, in 2018, Xu and co-workers[87] demonstrated two ESIPT-based fluorescent probes **2** and **3** for formaldehyde sensing in PBS buffer solution containing EtOH and DMSO (v/v/v = 50/50/0.1, 10 mM, pH 7.4) at 25 °C. Probe **2** showed two absorption bands at 300 and 365 nm. However, upon addition of formaldehyde, a notable decrease of the absorption intensity at 365 nm was observed, accompanied with a 5 nm blue shift. Due to the PET process between the amino group and benzothiazole, probe **2** exhibited weak emission at 519 nm. When formaldehyde was added to a solution of **2**, the emission band of the free probe at 519 nm (quantum yield: 0.098) displayed a significant fluorescence enhancement and gradual blue shift to 476 nm (quantum yield: 0.156). The fluorescence intensity of probe **2** at 476 nm increased linearly with the formaldehyde concentration from 0.5 to 2 mM. Similarly, the addition of formaldehyde to probe **3** led to the fluorescence enhancement at 486 nm, and the quantum yield changed from 0.085 (**3**) to 0.089 (**3** + formaldehyde). The detection limits of probe **2** and **3** for sensing formaldehyde were calculated to be 2 μM and 29 μM, respectively. The authors also developed test strips using probe **2** for rapid naked-eye detection of formaldehyde. Moreover, probe **2** was applied for imaging formaldehyde in MCF-7 cells as well as in *Arabidopsis thaliana* tissues (Fig. 2).

BODIPY-based formaldehyde chemodosimeter **4** was developed by Cao *et al.*[88] The spectral properties of this probe were tested in MeCN/HEPES buffer solution (1 : 9, v/v, 20 mM, pH 7.4). In the presence of formaldehyde, probe **4** causes a decrease in the absorption peak at 482 nm, along with an increase in the peak at 525 nm. Upon gradual addition of formaldehyde to the solution of **4**, a significant red shift in fluorescence is observed from 525 nm to 548 nm, accompanied by a dramatic fluorescence enhancement. The authors reported test kit experiments for the detection of hydrazine in environmental samples. Probe **4** had a detection limit of 0.104 μM and showed high selectivity over other potentially interfering analytes. Importantly, **4** was used to monitor and image formaldehyde in HeLa cells.

In the same year, Mahapatra's group[89] constructed a NBD (7-nitrobenz-2-oxa-1,3-diazole) piperazine conjugate **5** which showed a "turn-on" fluorescence response to formaldehyde. Upon addition of formaldehyde, probe **5** exhibited a decrease in absorption intensity at 485 nm, and the color of the solution turned from orange to yellow. In absolute aqueous HEPES buffer (pH 7.4) solution, only formaldehyde induced a large fluorescence enhancement at 545 nm (51-fold); meanwhile, other potential interferences such as reactive carbonyl and oxygen species (acetone, glucose, OCl^-, H_2O_2), other aliphatic and aromatic aldehydes (glyoxal, methylglyoxal, *p*-nitrobenzaldehyde, acetaldehyde, *p*-hydroxybenzaldehyde) and biothiols (cysteine, homocysteine and glutathione) did not elicit any noticeable changes, except that glyoxal responded slightly to probe **5**. The measured rate constant was 0.0107 s^{-1} for formaldehyde under pseudo-first-order conditions. The fluorescence intensity was linearly proportional to the concentrations of formaldehyde ranging from 0 to 2.5 μM with a low detection limit of 84 nM. Furthermore, probe **5** was used to detect formaldehyde in plywood samples and for fluorescence imaging of formaldehyde in living HADF cells.

In 2018, Jiang's group[90] devised a AIE-based turn-on probe (**6**) for formaldehyde based on an imine formation reaction. Initially, the probe was non-fluorescent in PBS solution (supplemented with 10% DMSO). However, on addition of formaldehyde, the fluorescence intensity was gradually enhanced at 530 nm (12-fold). The fluorescence intensity (λ_{em} = 530 nm) displayed a linear relationship toward concentrations of formaldehyde ranging from 100 nM to 1 μM, with a calculated detection limit of 40 nM. Cytotoxicity experiments in HeLa cells revealed that probe **6** had good biocompatibility. This probe was able to detect formaldehyde in living HeLa cells using confocal microscopy (Fig. 3).

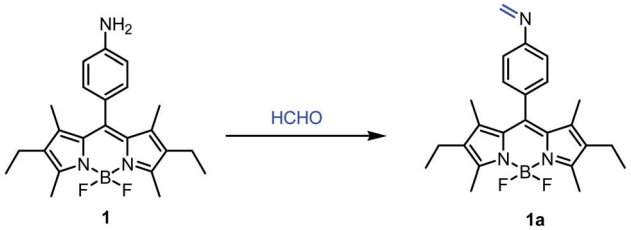

Fig. 1 Chemodosimetric reaction of probe **1** with formaldehyde.

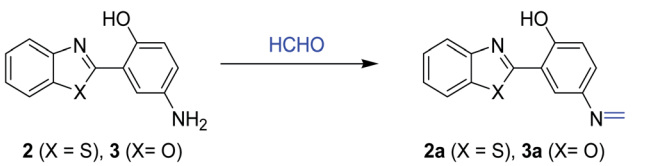

Fig. 2 Chemodosimetric reaction of probes **2** and **3** with formaldehyde.

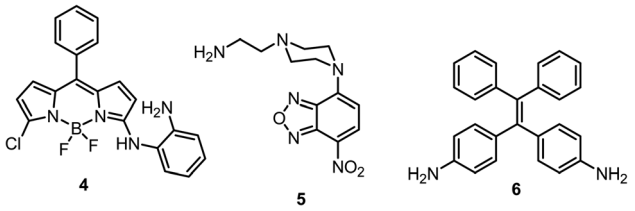

Fig. 3 Structures of formaldehyde probes 4–6.

In the next year, Hidayah *et al.*[91] designed amine group-containing pyridine-based fluorescent probe 7, which showed good sensitivity towards formaldehyde. The spectral studies of probe 7 were performed in acetonitrile solvent. Upon addition of aqueous solution of formaldehyde to the probe in acetonitrile, the emission wavelength shifted from 526 nm to 480 nm, accompanied by a sharp emission color change from yellow to blue which could be observed by the naked eye. This fluorescence change was mainly due to the formation of an imine bond (**7a**) by the reaction between the primary amine functional group and formaldehyde, resulting in inhibition of the PET process (Fig. 4). The detection limit of 7 for formaldehyde based on its fluorescence response is 0.58 mM, showing the high sensitivity of the probe. Importantly, an easy-to-prepare test kit was devised by the authors for the qualitative detection of formaldehyde in food samples.

Very recent work involving this strategy was reported by Cheng *et al.*[92] This probe (**8**) showed selective and sensitive fluorescence enhancement at 582 nm accompanied by a color change from purple to yellow due to formaldehyde, which was not observed for other biologically relevant analytes. The detection limit for formaldehyde was determined to be 1.5 μM in aqueous solution. Probe **8** was employed to detect formaldehyde in living HeLa cells.

In 2019, Chen *et al.*[93] described chemodosimetric fluorescent probes (**9–11**) for formaldehyde sensing. Among them, probe **9** exhibited higher selectivity and sensitivity toward formaldehyde than two control probes (**10** and **11**). Probe **10** displayed less selectivity toward formaldehyde, whereas probe **11** did not show fluorescence emission in presence of formaldehyde owing to the absence of the ICT effect. Upon the addition of formaldehyde to a PBS (pH 7.4, 1% DMSO) solution of **9**, the emission band of the free probe at 510 nm demonstrated a noteworthy fluorescence enhancement (14-fold) due to the ESIPT and ICT effects. The detection limit for formaldehyde was determined to be 0.35 μM. In contrast, other biologically relevant analytes displayed no apparent changes in the emission intensity of probe **9**. This probe was successfully employed in the fluorescence imaging of endogenous and exogenous formaldehyde in living cells.

In 2020, Wechakorn and co-workers[94] reported a colorimetric chemodosimeter **12**, which demonstrated excellent selectivity and sensitivity towards formaldehyde. Probe **12** displayed obvious absorption changes from 475 nm to 582 nm in the presence of formaldehyde in DMSO/KHP buffer (50% v/v, pH 4.0) solution with an apparent color change from yellow to deep purple, permitting naked eye formaldehyde detection. The sensing mechanism was established by ^{1}H NMR, ^{13}C NMR, and mass spectroscopy. In addition, the authors developed test strips containing probe **12** for detection of formaldehyde in aqueous medium (Fig. 5).

Ding *et al.*[95] introduced PET and FRET-based ratiometric fluorescent probe **13** for the detection of formaldehyde *via* an imine formation reaction. Initially, chemodosimeter **13** exhibited an emission peak at 426 nm. However, a significant decrease in the emission intensity at 426 nm was caused by the addition of formaldehyde to the probe's solution, followed by an increase in the emission intensity at 550 nm and a remarkable color change from blue to yellow. The fluorescence intensity ratios (I_{550}/I_{426}) established a good linear relationship with concentrations of formaldehyde ranging from 0 to 12.0 μM, and the detection limit of **13** for formaldehyde was calculated to be 8.3 ± 0.3 nM. This type of optical change was mainly due to the formation of yellow fluorescent product **13a** followed by the deactivation of PET and activation of FRET processes. Probe **13** was successfully applied in detecting formaldehyde in real food samples (dried fish, frozen shrimp, frozen small octopus, and frozen chicken). Additionally, probe **13** was able to visualize formaldehyde in living HeLa cells, onion epidermal tissues and living zebrafish (Fig. 6).

2.1.2. Hydrazine moiety-based chemodosimeters. Similarly, hydrazine moiety with an amino group was considered for formaldehyde sensing because of its strong nucleophilicity. It can instinctively react with carbonyl compounds and provide

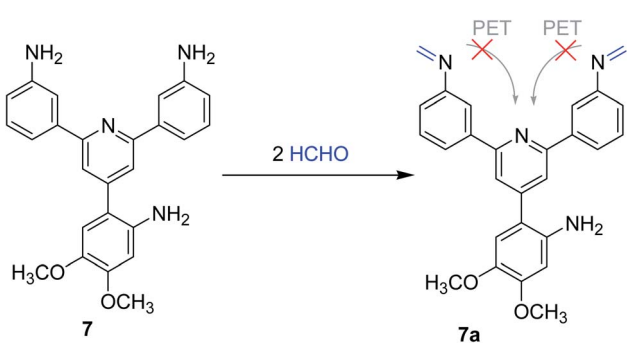

Fig. 4 Reaction of chemodosimeter 7 with formaldehyde.

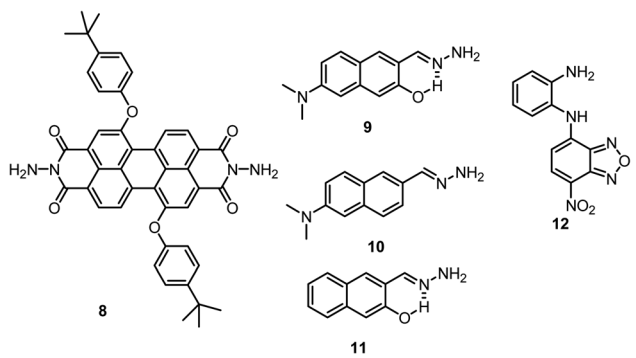

Fig. 5 Structures of formaldehyde probes 8–12.

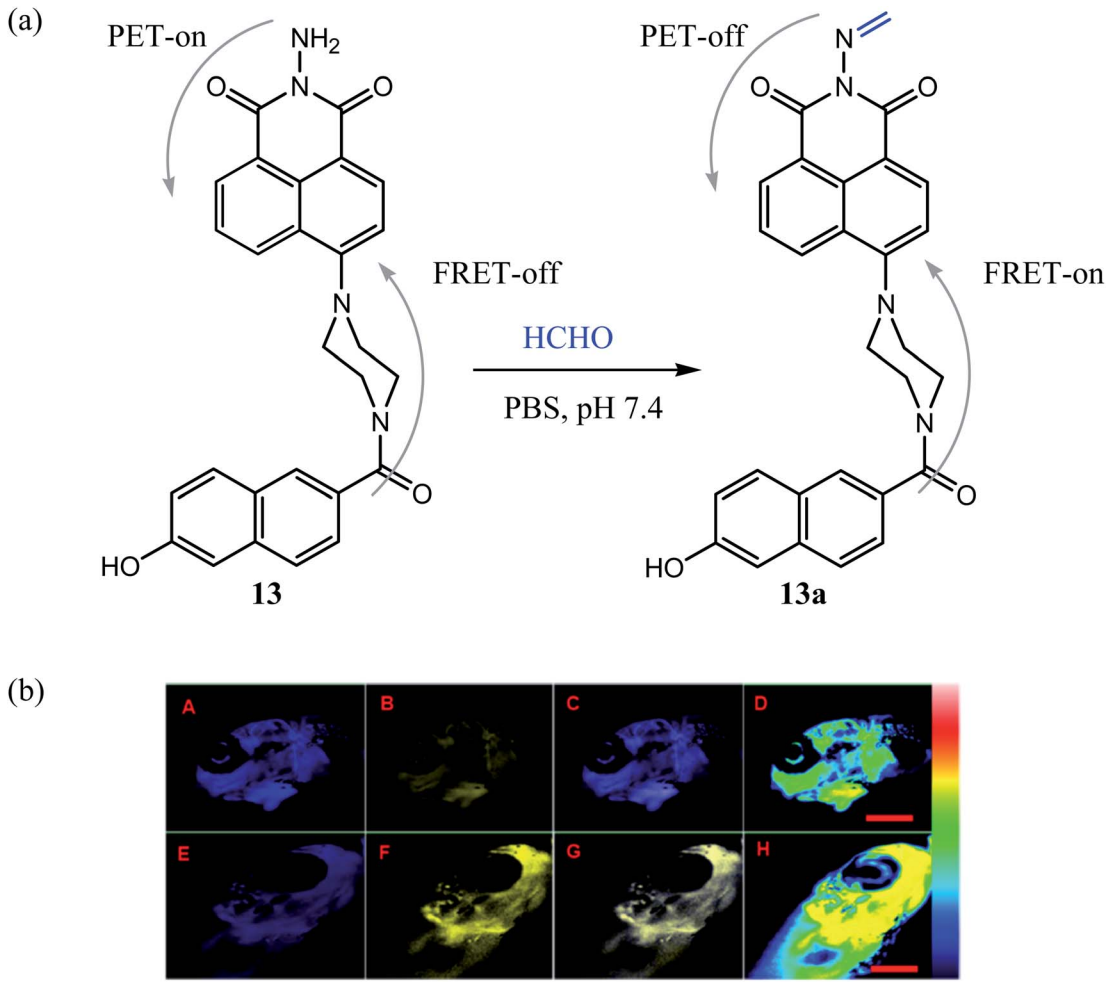

Fig. 6 (a) Reaction of chemodosimeter **13** with formaldehyde. (b) Fluorescent imaging of endogenous formaldehyde in living zebrafish [A–D (probe only) and E–H (probe + formaldehyde)]. Reprinted (adapted) with permission from ref. 95 Copyright (2020) American Chemical Society.

methylene hydrazine, which in turn helps to disrupt the PET process from the hydrazine functionality to the fluorophore (Scheme 2). In last few years, numerous fluorescent probes have been developed based on this approach.

Yu *et al.*[96] first reported the sensing of formaldehyde in aqueous ethanolic (1 : 1) solution utilizing hydrazine moiety-based chemodosimeter **14**. Due to the PET mechanism from aniline to the quinoline fluorophore, probe **14** displayed weak fluorescence at 467 nm in organo-aqueous solution. The fluorescence of **14** enhanced 5.5-fold in the presence of formaldehyde, which was due to the removal of the PET effect. The emission intensity revealed an excellent linear relationship with formaldehyde concentrations varying from 0 to 1.3 × 10^{-4} M, and a detection limit of 900 nM was estimated. Moreover, various carbonyl compounds such as formic acid, acetic acid, acetone, aldehyde, and propylaldehyde did not induce any interference. Probe **14** could be used to detect residual formaldehyde in various foods, such as fish slices, silk squid, yuba and dry seaweed. In addition, detection of formaldehyde on electrospinning nanofibers was described by the authors (Fig. 7).

Recently, a novel hydrazine-functionalized Al(III)-based MOF (**15**) was employed for the selective detection of formaldehyde in

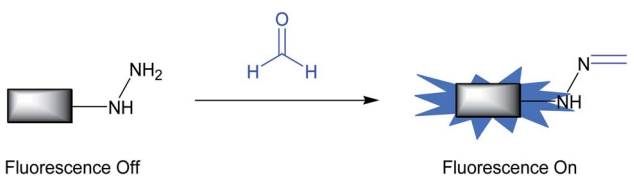

Scheme 2 Formaldehyde-selective fluorescent probes based on the Schiff base reaction.

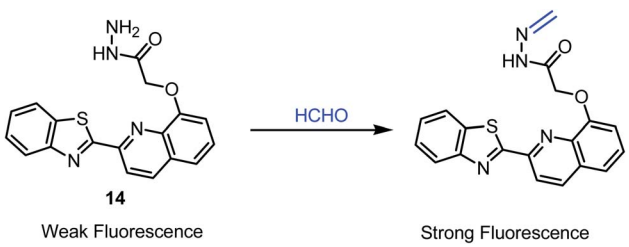

Fig. 7 Reaction of chemodosimeter **14** with formaldehyde.

aqueous media, HEPES buffer media, vapor phase, and live cancer cells.[97] The sensing nature of the probe can be attributed to the PET process. In the presence of formaldehyde, an imine formation reaction takes place, which caused a turn-on fluorescent response of the probe **15** (Fig. 8) because of the inhibition of the PET process from the hydrazine group to the phenyl ring. In HEPES buffer medium, a four-fold fluorescent enhancement was observed within 60 s after formaldehyde addition. This probe was used to sense formaldehyde selectively over another relevant aldehyde, with a detection limit of 8.37 μM (0.25 ppm) in HEPES buffer medium and 2.14 μM (64.33 ppb) in aqueous medium. The authors reported that this probe was also able to image formaldehyde in MDAMB-231 breast cancer cells, suggesting the real application of probe **15** in the analysis of biological samples (Table 1).

In 2018, Lin and co-workers[98] developed another 1,8-napthalimide-based two-photon fluorescent probe **16** for selective formaldehyde detection, which contained a hydrazine moiety as the reactive unit for formaldehyde. In the presence of formaldehyde, probe **16** displayed turn-on fluorescence response at 539 nm in 10 mM PBS buffer (pH 7.4, containing 5% DMSO as co-solvent) solution, as the condensation reaction between the hydrazine moiety of **16** and formaldehyde could prevent the PET mechanism. The emission intensity at 539 nm was linearly proportional to the concentration of formaldehyde (0–50 μM), and the detection limit was found to be 4.9×10^{-6} M. Moreover, the chemodosimeter has high selectivity and can be successfully applied to image endogenous formaldehyde in living HeLa cells and living mice liver tissue slices.

Using the same strategy, in 2018, Li *et al.*[99] reported a hydrazino-naphthalimide-functionalized chitosan-based turn-on polymeric probe (**17**) for selective, sensitive and ultrafast detection of formaldehyde in aqueous solution. This sensor displayed high sensitivity toward formaldehyde, with a detection limit as low as 0.05 ppm (1.66 μM). Additionally, this sensor was successfully employed to detect formaldehyde in real water and food samples.

Recently, Song and co-workers[100] designed a BODIPY-based turn-on fluorescent chemodosimeter (**18**) for sensing of formaldehyde with high selectivity over other competitive species. Probe

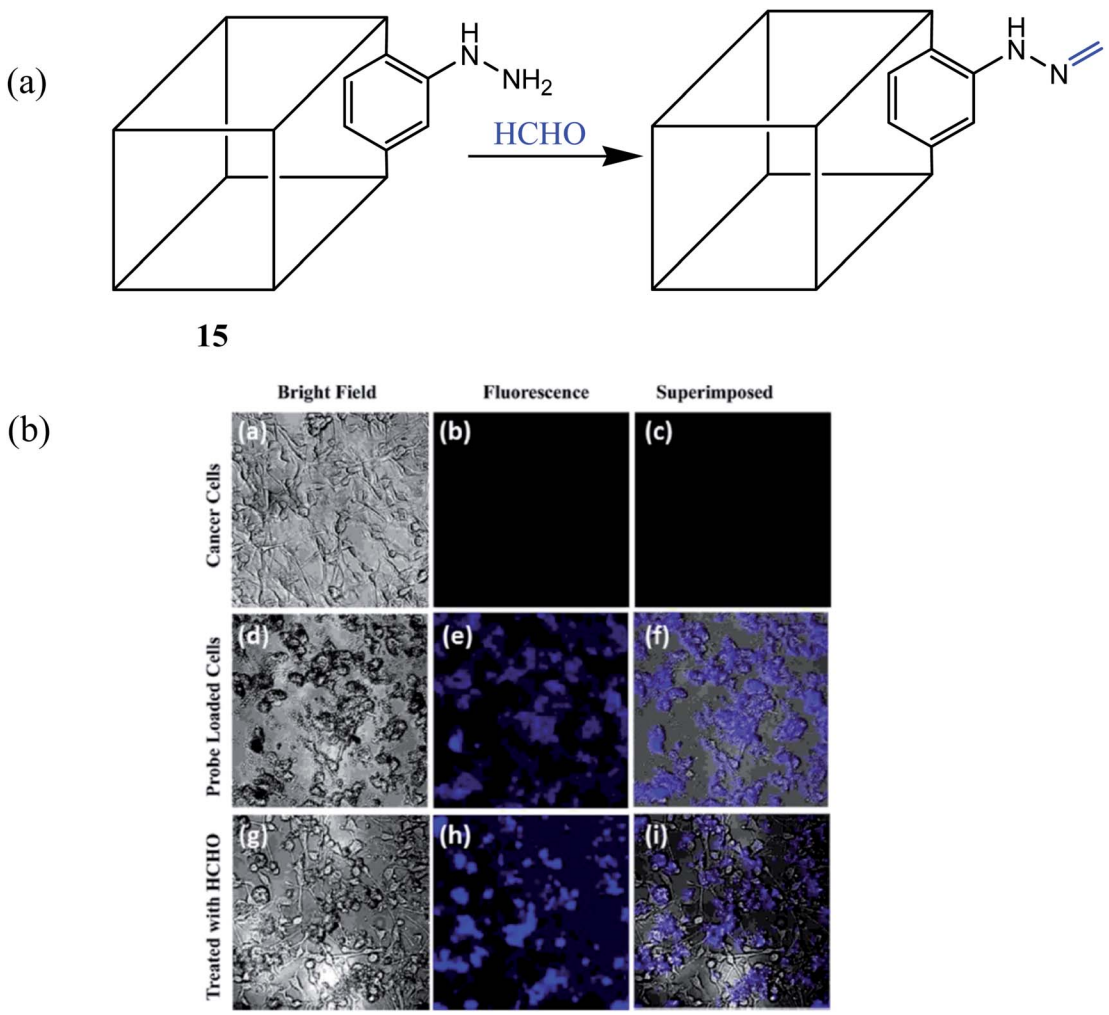

Fig. 8 (a) Reaction of probe **15** with formaldehyde. (b) Fluorescence images of MDAMB-231 breast cancer cells. Reprinted (adapted) with permission from ref. 97 Copyright (2018) American Chemical Society.

Table 1 Summary and comparison of the photophysical properties of formaldehyde selective chemodosimeters **1–56**

Chemodosimeter (fluorophore)	Nature of the probe/ photophysical mech.	Solvent	λ_{ex} (nm)	λ_{em} (nm)	Quantum yield (Φ) in absence/ presence of HCHO	Detection limit/ linear range	Time	Applications	Ref.
1 (BODIPY)	Turn-on/PET	CH_3OH (pH 8.0)	520	535	0.05/—	165 nM/—	—	—	86
2 & **3** (benzothiazole & benzoxazole)	Turn-on/PET, ESIPT	PBS buffer solution containing EtOH and DMSO (v/v/v = 50/50/0.1, 10 mM, pH 7.4)	360	519 to 476 (**2**), 486 (**3**)	0.098/0.156 (**2**), 0.085/0.089 (**3**)	2 μM (**2**), 29 μM(**3**)/ 0.5–2 mM (**2**)	Less than 3 min	Test strips, cell imaging (MCF-7 cells & *Arabidopsis thaliana* root tip tissues) (**2**)	87
4 (BODIPY)	Turn-on/ICT	MeCN/HEPES buffer (1 : 9, v/v, 20 mM, pH 7.4)	482	525 to 548	(0.016 ± 0.0022)/ (0.252 ± 0.0310)	0.104 μM/0–1000 μM	90 min	Cell imaging (HeLa cells), test papers	88
5 (NBD)	Turn-on/PET	Absolute aqueous HEPES buffer	485	545	0.0108/0.5608	84 nM/0–2.5 μM	2 min	Cell imaging (HADF cells), test kits (plywood samples)	89
6 (tetraphenyl ethylene)	Turn-on/AIE	PBS, supplemented with 10% DMSO	370	530	—	40 nM/100 nM to 1 μM	~90 s	Cell imaging (HeLa cells)	90
7 (tri aryl pyridine)	—/PET	Acetonitrile	363	526 to 480	—	0.58 mM/0–1.4 M	65 min	Paper strips (food samples)	91
8 (perylenebisimide)	Turn-on/PET	THF/H_2O (v/v, 1/3)	540	582	0.02/0.62	1.5 μM/2–10 μM	Within 1 min	Cell imaging (HeLa cells)	92
9–11 (naphthalene)	Turn-on/ICT, ESIPT	PBS (pH 7.4, 1% DMSO)	405 (**9**)	510 (**9**)	—	0.35 μM/1.0–500 μM (**9**)	100 min (**9**)	Cell imaging (HeLa cells) (**9**)	93
12 (–)	Colorimetric (ratiometric)/—	DMSO/KHP buffer (50% v/v, pH 4.0)	475 to 582	—	—	30 μM/0–6.5 mM	30 min	Paper strips	94
13 (1,8-naphthalimide)	Ratiometric/PET, FRET	10 mM PBS, $V_{DMSO/PBS} = 1/99$	385	426 to 550	—	8.3 ± 0.3 nM/0–12.0 μM	Within 1 min	Cell imaging (live HeLa cells, onion tissues, and zebra fish), real food samples	95
14 (benzothiazole–quinoline)	Turn-on/PET	$V_{water} : V_{ethanol} = 1 : 1$	350	467	—	900 nM/0–1.3 × 10^{-4} M	—	Food samples (fish slices, silk squid, yuba and dry sea weed) and electrospinning test strips	96
15 Al(III) based MOF	Turn-on/PET	HEPES buffer & aqueous media	330	436	—	8.37 μM (0.25 ppm) (HEPES), 2.14 μM (64.33 ppb) (aqueous)/—	60 s	Cell imaging (MDAMB-231), probe-coated quartz slide for vapor phase sensing	97
16 (1,8-naphthalimide)	Turn-on (two-photon)/PET	PBS buffer (pH 7.4, 5% DMSO)	440	539	—	4.9 × 10^{-6} M/0–50 μM	40 min	Cell imaging (HeLa cells & mice liver tissues)	98

Table 1 (*Contd.*)

Chemodosimeter (fluorophore)	Nature of the probe/ photophysical mech.	Solvent	λ_{ex} (nm)	λ_{em} (nm)	Quantum yield (Φ) in absence/ presence of HCHO	Detection limit/ linear range	Time	Applications	Ref.
17 (1,8-naphthalimide)	Turn-on/PET	Aqueous solution	440	555	—	0.05 ppm (1.66 μM)/1–100 ppm	Less than 1 min	Real world food and water samples	99
18 (BODIPY)	Turn-on/TICT, ICT	PBS buffer (1% DMSO, pH 7.4),	420	466	—/0.40	0.18 μM/0–100 μM	<30 min	Cell imaging (HeLa cells)	100
19 (1,8-naphthalimide)	Turn-on (two-photon)/PET	10 mM PBS buffer (pH 7.4)	440	550	0.051/0.326	12.4 μM/0–50 μM	Within 20 min	Cell imaging (HeLa cells & zebra fish)	101
20 (1,8-naphthalimide)	Turn-on (two-photon)/PET	10 mM PBS (pH 7.4)	440	550	0.088/0.266	1.62×10^{-6} M/0–10 μM	Within 20 min	Live cell imaging (HeLa cells), milk samples	102
21 (2,5-dihydroxy-*p*-benzenedicarbonamide)	Ratiometric/PET, ICT	PBS buffer (pH = 7.4)	385	508 to 534	0.027/0.055	0.29 μM	13 min	Live cell imaging (HeLa cells), test papers	103
22 (NBD)	Turn-on/PET	—	470	550	—	0.89 μg L^{-1}/0.015–0.8 mg L^{-1}	40 min	Real sample analysis	104
23 (1,8-naphthalimide)	Turn-on/PET	DMSO : PBS = 1 : 1 (v/v, pH = 7.4)	417	519	—	0.36 μM/0–100 μM	Within 8 s	Cell imaging (MCF-7 cells)	105
24 (rhodamine–napthalimide)	Turn-on/PET	Tris–HCl buffer solution containing 30% EtOH (10 mM, pH 7.4)	440	534	0.006/0.13	0.21 μM/0–120 μM	Within 5 min	Cell imaging (HeLa cells & zebrafish), real sea food samples analysis	106
25 (julolidine-based silicon rhodol)	Turn-on/PET	PBS buffer (pH 7.4) at 37 °C	633	649	—	—	—	Cell imaging (live HEK293TN & Neuroscreen-1 cells.)	109
26 (1,8-naphthalimide)	Turn-on/PET, ICT	PBS buffer (25 mM, pH 7.4, containing 20% DMSO)	395	518	0.032/0.341	0.22 μM/10–350 μM	180 min	Cell imaging (HeLa cells)	110
27 (tetraphenyl ethylene)	Turn-on/PET, AIE	DMSO/H_2O (v/v, 1 : 9)	335	480	2.64%/35.42% (solid state)	0.036 mg m^{-3}/0–1.6 mg m^{-3}	60 min	Test plates for gaseous formaldehyde detection	111
28 (pyrene)	Turn-on/—	EtOH/HEPES (10 mM, pH = 7.4, 1 : 99, v/v)	390	472	—	0.107 μM)/0–10 μM	—	Live cell imaging (HEK293T cells)	112
29 (NBD)	Turn-on/ICT	HEPES buffer containing DMSO (v/v = 1 : 1, 20 mM, pH 7.4)	460	578	0.015/0.080	9.7 μM/0 to 0.8 mM	3 h approximately	Cell imaging (MCF-7), kidney tissues of mice, *Daphnia magna*	113
30 (benzooxadiazole)	Turn-on/ICT	PBS buffer (25 mM, pH 7.4, containing 20% MeCN)	470	563	0.0032/0.0615	4.35×10^{-8} M and 4.97×10^{-8} M (S/N = 3) for low and high concentration levels/(0–100 μM and 200–500 μM)	180 min	Cell imaging (HeLa cells)	114

Table 1 (*Contd.*)

Chemodosimeter (fluorophore)	Nature of the probe/ photophysical mech.	Solvent	λ_{ex} (nm)	λ_{em} (nm)	Quantum yield (Φ) in absence/ presence of HCHO	Detection limit/ linear range	Time	Applications	Ref.
31 (quinoline)	Ratiometric/ICT	PBS solution (pH 7.4, 10 mM)	355	405 to 490	—	4.054 μM/0–1.0 mM	—	Cell imaging (MCF-7 cells, mice liver tissue and 5 days old zebra fish)	115
32 & **33** (–)	Turn-on/—	PBS (10 mM, pH 7.4, 10% FBS)	—	540 (**32**), 700 (**33**)	—	—/—	60 min	Cell imaging (HEK293 cells) (**32**), living mice (**33**)	116
34 (1,8-napthalimide)	Turn-on/—	PBS buffer (0.5% DMSO, 10 mM)	455	555	—	10 μM/0–0.25 mM	25 min	Cell imaging (HeLa cells)	117
35 (benzothiazole)	Turn-on/PET	PBS buffer–CH_3CN (10 mM, pH 7.4, 7 : 3, v/v)	350	542	—	2.5×10^{-4} M/0–10 mM	3 hours	Vapour phase detection by test papers	118
36 (perylene)	Ratiometric/—	DMSO solution & aqueous solution (nanoprobe)	420 (DMSO) & 450 (nano probe)	452 to 550 (DMSO) 480 to 550 (nano probe)	—	6.1 μM (DMSO) & 0.96 μM (nanoprobe)/0–0.8 mM (DMSO) & —	90 min (DMSO) & 120 min (nano probe)	Cell imaging (HeLa cells) (nano probe)	119
37 [4-(diphenylamino) phenyl moiety]	Ratiometric/AIE, ICT	1,4-Dioxane/water (2 : 8, v/v)	305	442 to 488	—	5.1×10^{-5} M/0–5.6 mM	80 min (solution), 45 min (test cotton)	Fabric and cotton samples	120
38 (Ru(II)-complex)	Turn-on/PET	50 mM HOAc/OAc– buffer at pH 5.0	460	644	0.10%/2.12%	19.8 nM/0 to 650 μM	120 min	Cell imaging [HeLa cells, mice (*in vivo* & *in vitro*)], test strips, human serum samples	121
39 (coumarin)	Turn-off/ICT	PBS (pH = 7.4, 5% DMSO)	405	451	0.921/0.0713	4.16×10^{-5} M/0–20 μM	200 min	Cell imaging (HeLa cells, zebra fish, liver tissue of zebra fish)	122
40 (benzothiazole)	Ratiometric/—	Phosphate buffer : DMSO = 1 : 1 (v/v, pH 7.4, 10 mM)	430	492 to 552	0.23/0.16	0.58 μM/0–500 μM	90 min	Cell imaging (MGC-803 cells, zebra fish), water samples	123
41–45 (quinoline)	Turn-on/ICT, TICT	PBS buffer (10 mM, pH 7.4, containing 1% MeCN)	355 (**41**), 386 (**42**), 346 (**43**), 400 (**44**), 355 (**45**)	571 (**41**), 567 (**42**), 512 (**43**), 508 (**44**), 526 (**45**)	0.23/0.72 (**41**), 0.21/ 0.54 (**42**), 0.21/0.51 (**43**), 0.20/0.60 (**44**), 0.42/0.66 (**45**)	0.3 μM/0–2 mM (**41**)	3 h (**41**)	Cell imaging (live *C. elegans*) (**41**)	124
46 (carbazole)	Ratiometric/ICT	H_2O/DMSO mixture (3/7, v/v)	366	393 to 542	—	1.55 μM/10 to 800 μM	30 s (solid state), 3 h (solution)	Cell imaging (HeLA cells), test strips	125
47 (Zn-MOF)	Turn-on/—	DMF and Tris buffer solution (7 : 3, v/v),	380	438	—	2.3 μM/0–25 mM	28 s	Test papers	126
48 & **49** (–)	Turn-on/—	MeOH	300	545	—	0.10 μM & 100 nM (paper strips)/—	—	Paper strips	127

Table 1 (*Contd.*)

Chemodosimeter (fluorophore)	Nature of the probe/ photophysical mech.	Solvent	λ_{ex} (nm)	λ_{em} (nm)	Quantum yield (Φ) in absence/ presence of HCHO	Detection limit/ linear range	Time	Applications	Ref.
50 (dopamine)	Turn-on/—	Phosphate buffer (pH = 8)	420	485	—	0.24 mM (sol) and 0.7 ppm (gas)/0.5 to 67 mM	Within 2 min (color change)	Test strips	129
51 (dansyl–benzopyrylium)	Ratiometric/FRET	PBS buffer (20% CH_3CN)	365	550 to 635	—	—	—	Cell imaging (HeLA cells and living mouse)	130
52 & **53** (carbazole–benzopyrylium)	Ratiometric/—	10 mM HEPES buffer (20% CH_3CN)	370 (**52**), 270 (**53**)	425 to 635 (**52**), 370 to 630 (**53**)	—	—	Less than 1 min (**53**)	Cell imaging (living HeLa cells, living zebra fish and murine species) (**53**)	131
54 & **55** (squarine)	Colorimetric & fluorometric/—	Aqueous solution	640 (**54**), 616 (**55**)	667 (**54**)	—	60 μM (from fluorescence titration)/— (**54**)	Less than 1 s	—	132
56 (heptamethine cyanine derivative)	Colorimetric/—	MeOH	720	800	—	3.25 μM/0–1.2 mM	Within 30 s	Test papers	133

18 was able to detect formaldehyde *via* a color change and a fluorescence change. This probe is non-fluorescent in PBS buffer due to the twisted intramolecular charge transfer (TICT) process from the strong electron-donating hydrazine group to the BODIPY unit. In the presence of formaldehyde, the hydrazine moiety of **18** is transformed to the hydrazone moiety, a process that brings about a >900-fold fluorescence enhancement at 466 nm, accompanied by a color change from colorless to blue. The detection limit for formaldehyde was calculated to be 0.18 μM, and a linear relationship between the emission intensity and formaldehyde concentration was found to exist in the range of 0–100 μM. In addition, chemodosimeter **18** showed a fluorescence turn-on response to formaldehyde in living HeLa cells.

Using the same imine formation strategy, Zhang and co-workers[101] designed and synthesized a two-photon fluorescent probe (**19**) for formaldehyde detection based on the PET mechanism. Initially, probe **19** showed a weak emission band (Φ = 0.051) due to the PET effect. However, addition of formaldehyde to the PBS (10 mM, pH 7.4) solution of **19** deactivated the internal PET mechanism and led to a 12-fold fluorescence enhancement at 550 nm (Φ = 0.326) with a detection limit of 12.4 μM. The fluorescence intensity showed a good linear relationship with formaldehyde concentration ranging from 0 to 50 μM. Several carbonyl compounds, including some nucleophilic species such as amino acids, anions, reactive oxygen species, reactive nitrogen species, ketones and aldehydes, did not show any remarkable emission changes. In addition, it was found that probe **19** could be used to image formaldehyde in Hela cells and zebrafish. Moreover, monitoring of mitochondrial damage caused by formaldehyde stress was reported by the authors.

Very recently, Zhang and co-workers[102] employed the imine formation approach to design a two-photon fluorescent chemodosimeter (**20**) for formaldehyde. The free probe **20** was weakly fluorescent (Φ = 0.088) in PBS (pH 7.4) solution. However, upon addition of formaldehyde, the fluorescence intensity was gradually enhanced due to formation of fluorescent hydrazone (Φ = 0.266). Confocal microscopy experiments confirmed that **20** was able to sense formaldehyde in living HeLa cells. In addition, the author demonstrated that this probe was capable of sensing basal formaldehyde in milk samples (Fig. 9).

Probe **21** was designed for the selective and sensitive detection of formaldehyde assisted by an imine formation reaction.[103] Probe **21** demonstrated weak fluorescence at 508 nm (Φ = 0.027) in PBS buffer (pH 7.4) solution due to ICT and the PET quenching process. However, upon gradual addition of formaldehyde to the solution of **21**, red shift of fluorescence emission was observed from 508 nm to 534 nm, resulting in a fluorescence color change from light green to bright yellow-green. Moreover, the probe **21** was used to selectively detect formaldehyde in living HeLa cells. Additionally, probe **21** was employed for gaseous formaldehyde detection using test papers.

Hongwei *et al.*[104] reported a chemodosimeter (**22**) that underwent fluorescence changes upon reaction with formaldehyde. Fluorometric titration of **22** with formaldehyde resulted in fluorescence enhancement at 550 nm. Chemodosimeter **22**

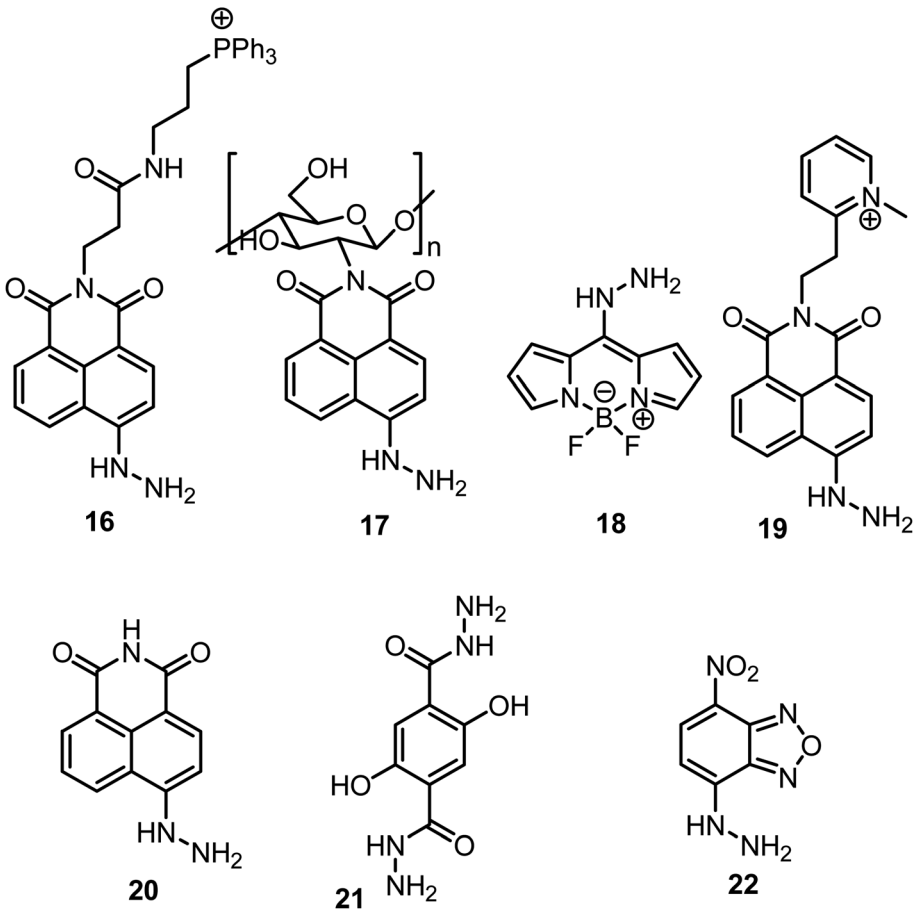

Fig. 9 Structures of formaldehyde probes **16–22**.

displayed a low detection limit of 0.89 μg L^{-1} and functioned well over an extensive linear range of 0.015–0.8 mg L^{-1}. The sensing mechanism is due to the imine formation reaction between formaldehyde and the primary amine group of the probe, which caused inhibition of the PET process. The authors reported test paper strip experiments for monitoring formaldehyde in different water samples.

Wang and coworkers[105] reported a naphthalimide-based probe **23** that was used for the highly selective and sensitive detection of formaldehyde in DMSO : PBS (1 : 1, v/v, pH 7.4) solution. Initially, probe **23** showed weak fluorescence in the absence of formaldehyde in DMSO : PBS solution. When formaldehyde was added to the solution of **23**, a significant fluorescence enhancement at 519 nm was observed due to the inhibition of the PET mechanism (Fig. 10). Probe **23** displayed a highly linear relationship with the concentration of formaldehyde in the range of 0–100 μM and a detection limit of 0.36 μM. Several analytes, such as benzaldehyde, oxalaldehyde, *p*-hydroxybenzaldehyde, *p*-chlorobenzaldehyde, 2,4-dihydroxybenzaldehyde, *p*-hydroxyacetophenone, Cys, Hcy, Gsh, Na^+, K^+, Ca^{2+}, Ba^{2+} and Mg^{2+}, did not induce any noticeable emission spectral changes. Upon addition of formaldehyde, the initial absorption peak at 449 nm was blue shifted to 435 nm (isosbestic point 453 nm), and the color of the solution changed from dark red to bright yellow. In addition, cell imaging experiments revealed that probe **23** could be employed to image endogenous formaldehyde in MCF-7 cells.

Jiang *et al.*[106] reported a rhodamine derivative **24** as a fluorescent turn-on chemodosimeter for selective detection of formaldehyde in solution as well as in biological samples. Probe **24** was initially nonfluorescent ($\Phi = 0.006$) due to the PET process from the nitrogen of the hydrazine moiety to the naphthalimide unit; however, it showed a strong fluorescence

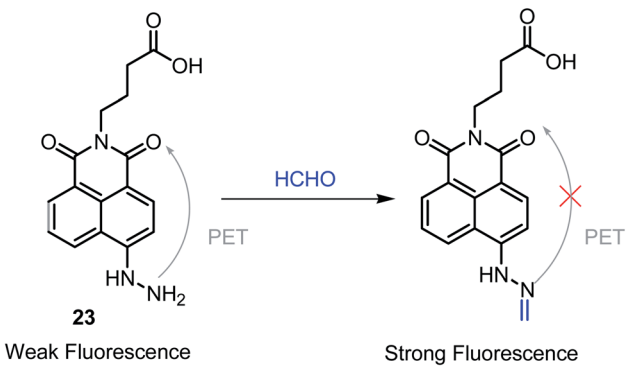

Fig. 10 Reaction of chemodosimeter **23** with formaldehyde.

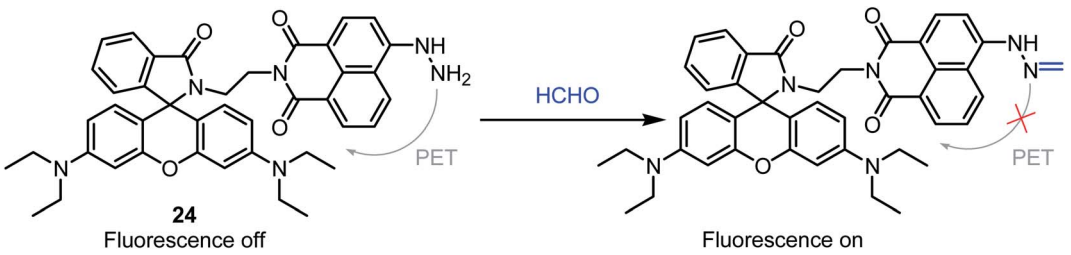

Fig. 11 Reaction of chemodosimeter **24** with formaldehyde.

enhancement ($\Phi = 0.13$) at 534 nm in the presence of formaldehyde due to deactivation of the PET mechanism (Fig. 11). Additionally, this apparent fluorescence enhancement showed a good linear relationship with the formaldehyde concentration in the range of 0–120 μM, and the detection limit for probe **24** was calculated to be 0.21 μM. Finally, the authors demonstrated that probe **24** was able to detect endogenous formaldehyde in HeLa cells and zebrafish. Moreover, probe **24** was employed to sense formaldehyde in real seafood, such as dried squid, fresh octopus A, and fresh octopus B.

Owing to their low cytotoxicity, amine/hydrazine derivatives attract tremendous attention from researchers for the development of formaldehyde-selective fluorescence probes. Advantageously, amine/hydrazine derivatives react instantaneously with formaldehyde with higher selectivity than other developed methods. In some case, Schiff base-based probes have been considered for quantification of metal ions.[107] To overcome any additional interference for the selective detection of formaldehyde, appropriate structural modifications are highly necessary, and researchers should screen a wider range of analytes in order to showcase the superiority of formaldehyde detection over others.

2.2. 2-aza-Cope sigmatropic rearrangement reaction

When a homoallylic amine group is attached to a probe, a 2-aza-Cope sigmatropic rearrangement reaction[108] can take place in the presence of formaldehyde. As shown in Scheme 3, at first, the amine group selectively reacts with formaldehyde to form an iminium intermediate ($\mathbf{I_1}$), which then concurrently undergoes a 2-aza-Cope rearrangement reaction ($\mathbf{I_2}$) and finally hydrolysis to yield a fluorescent aldehyde product (**P**), which changes the optical properties of the chemodosimeter. Here, we focus on several formaldehyde-selective chemodosimeters based on napthalimide, quinoline, pyrene, benzothiazole, naphthalene, metal complex, perylene nanoprobe platform, tetraphenyl ethylene (TPE), NBD derivative, benzooxadiazole, coumarin, carbazole and a metal–organic framework (MOF). In addition to this fluorescence turn-on mechanism, seven ratiometric fluorescence probes are also reported.

In 2015, Chan *et al.* first employed this technique to design a formaldehyde chemodosimeter.[109] The fluorescence of chemodosimeter **25** was strongly reduced by the d-PET process. However, in the presence of formaldehyde, excellent fluorescence was achieved owing to the formation of product **25a** ($\Phi = 0.11$); consequently, PET was obstructed. The detection limit for formaldehyde was 0.01 mM in PBS buffer solution. On the other hand, no substantial changes in the fluorescence intensity of **25** were shown by other competitive analytes. Again, this probe was fruitfully used in the confocal microscopic imaging of formaldehyde in live HEK293TN and NS1 cells in a dose- and time-dependent manner (Fig. 12).

Using this approach, Lin's group[110] reported naphthalimide-based fluorescent probe **26** for detection of formaldehyde in

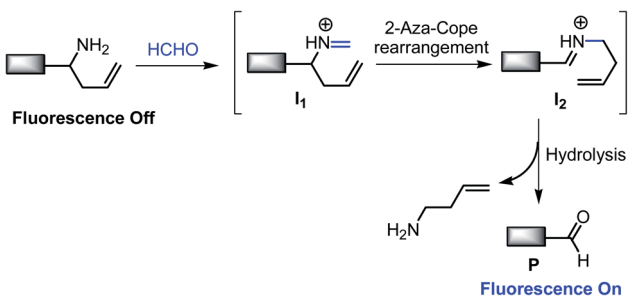

Scheme 3 Strategy for the design of formaldehyde-selective fluorescence probes based on a 2-aza-Cope rearrangement reaction.

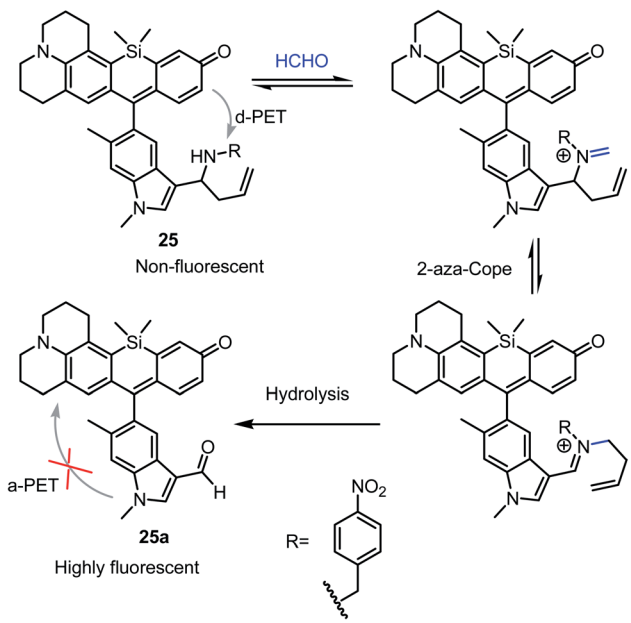

Fig. 12 Reaction of chemodosimeter **25** with formaldehyde.

solution as well as in living organisms. Initially, probe **26** was almost non-fluorescent. However, in the presence of formaldehyde, probe **26** reacted with formaldehyde and was converted into product **26a**, accompanied with a very strong turn-on fluorescence signal centered at 518 nm. The formation of the product **26a** was confirmed by HRMS spectra. Probe **26** showed high selectivity towards formaldehyde over other competitive analytes, such as 2-ethylacrolein, propanal, butyraldehyde, aldehyde, glyoxylic acid, isovaleral, methylglyoxal, oxalaldehyde, 2-ethylbutyraldehyde, glutaraldehyde, 3-methyl-2-butenal, H_2S, $S_2O_3^{2-}$, GSH, Arg, Glu, Ser, ClO^-, H_2O_2, TBHP, Ca^{2+}, K^+ and Zn^{2+}. The authors successfully demonstrated the utilization of this probe in living HeLa cells for monitoring the presence of formaldehyde (Fig. 13).

Zhao *et al.*[111] prepared an aggregation-induced emission-based probe **27** for the fluorescence turn-on detection of formaldehyde. Probe **27**, which initially has almost no fluorescence due to the PET effect, reacts rapidly with formaldehyde in DMSO/H_2O (v/v, 1 : 9) solution to form an aldehyde compound; this inhibits the PET process and results in a highly fluorescent compound. The authors developed a portable solid test plate for selective, sensitive and quantitative detection of gaseous formaldehyde (Fig. 14).

Zhang *et al.*[112] devised a pyrene derivative (**28**) containing homoallylamino moiety as a 'turn-on' fluorescent chemodosimeter for selective detection of formaldehyde in EtOH/HEPES (10 mM, pH 7.4, 1 : 99, v/v) solution. A significant emission enhancement at 472 nm was observed for probe **28** upon gradual addition of 20 equivalents of formaldehyde, with a detection limit of 0.107 μM. No interference from other analytes, including reactive carbonyl species (RCS) (benzaldehyde, *p*-anisaldehyde, methyl isothiocyanate, phenyl isothiocyanate, formic acid, 2-(diphenylphosphino)benzoic acid, glucose, acetone, *p*-nitrobenzaldehyde, methylglyoxal, sodium ascorbate, and acetaldehyde), reactive oxygen species (ROS) (ClO^-, H_2O_2), and thiol-containing compounds (HS^-, GSH, Cys and Hcy), was observed for the signaling of formaldehyde by chemodosimeter **28**. The probe **28** was cell permeable and hence was used for imaging formaldehyde in biological samples.

Yang *et al.*[113] used the fluorescent chemodosimeter **29** for the detection of formaldehyde based on the formation of an aldehyde compound *via* an aza-Cope rearrangement reaction. The

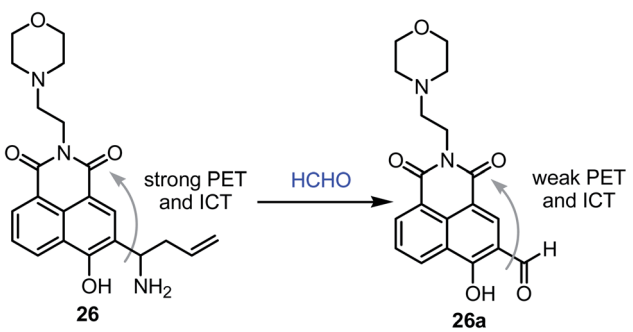

Fig. 13 Reaction of probe **26** with formaldehyde.

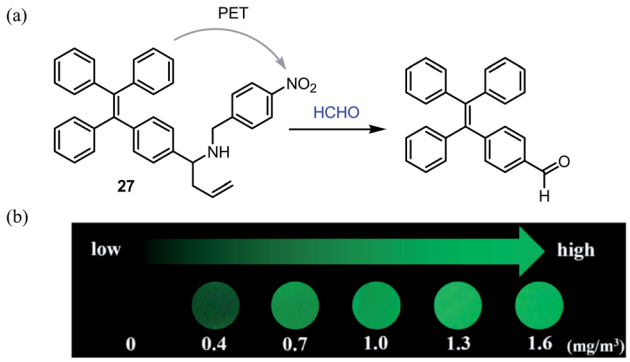

Fig. 14 (a) Reaction of probe **27** with formaldehyde. (b) Photographs of formaldehyde detecting plates taken under a UV lamp (365 nm) after 60 min incubation with several concentrations of gaseous formaldehyde. Reprinted (adapted) with permission from ref. 111. Copyright (2018) American Chemical Society.

optical response of probe **29** to several analytes was investigated in HEPES buffer containing DMSO (v/v = 1 : 1, 20 mM, pH 7.4) solution. The authors found that the reaction between probe **29** and formaldehyde resulted in noteworthy gradual fluorescence enhancement (55-fold) at 578 nm, and the fluorescence quantum yield of **29** increased from 0.015 to 0.080. The emission intensity displayed a good linear relationship with the formaldehyde concentration ranging from 0 to 0.8 mM, and the detection limit was found to be 9.7 μM. Probe **29** was cell permeable and was used for fluorescence imaging formaldehyde in living cells and kidney tissues of mice. Moreover, probe **29** was employed to monitor formaldehyde in living *Daphnia magna* for the first time.

In 2018, Lin and co-workers[114] implemented the same strategy to develop an ICT-based fluorometric chemodosimeter **30** for the selective detection of formaldehyde in solution as well as in living cells. In aqueous (25 mM PBS buffer, pH 7.4, containing 20% MeCN) solution, the addition of formaldehyde to probe **30** resulted in a 'turn-on' fluorescence response at 563 nm, which was suggested to be due to the formation of an aldehyde product. Further, the formation of the aldehyde product was confirmed by HRMS analysis and DFT studies. The measured rate constant was found to be 0.019 min^{-1} for formaldehyde. Probe **30** was effectively employed to visualize formaldehyde in living HeLa cells.

Ratiometric two-photon fluorescent probe **31**, based on a quinoline derivative, was reported for the highly selective and sensitive detection of formaldehyde.[115] Upon gradual addition of formaldehyde to the PBS buffer solution of **31** (10 mM, pH 7.4), the initial emission band of **31** at 405 nm gradually decreased with a concomitant increase in a new emission band at 490 nm, accompanied with a solution color change from blue to green. The ratio of the fluorescence intensities at 490 and 405 nm ($I_{490\ nm}/I_{405\ nm}$) increased linearly with the formaldehyde concentration from 0 to 1.0 mM, with a detection limit of 4.054 μM. The authors also demonstrated that this probe was competent to image endogenous formaldehyde in MCF-7 cells, living tissues and living 5 day-old zebrafish larvae (Fig. 15).

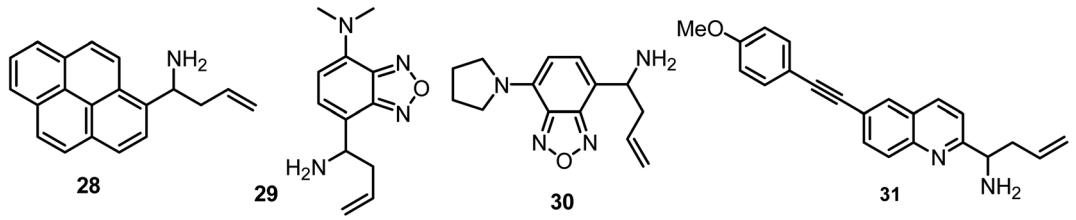

Fig. 15 Structures of formaldehyde probes **28**–**31**.

Recently, Chang and co-workers[116] designed two chemiluminescent probes (**32** and **33**) for highly sensitive and selective detection of formaldehyde. In the presence of formaldehyde, the probe underwent an aza-Cope rearrangement reaction followed by β-elimination to yield the free phenoxy-dioxetane, which subsequently released the emissive methyl ester compound *via* chemiexcitation, as shown in Fig. 16. With the addition of formaldehyde, probe **32** induced a 500-fold emission intensity increase, whereas **33** caused fluorescence enhancement by 33-fold when measured in PBS (10 mM, pH 7.4, 10% FBS, at 37 °C) solution. Moreover, biological studies confirmed that both probes **32** and **33** were effective for imaging formaldehyde levels in live HEK293 cells and mice, respectively.

Later, Xie *et al.*[117] reported 1,8-naphthalimide based chemodosimeter **34**, which sensed formaldehyde *via* a 2-aza-Cope rearrangement reaction followed by a β-elimination reaction (Fig. 17). It was proposed that in the presence of formaldehyde, probe **34** was converted to the corresponding 4-hydroxy-1,8-napthalimide, and its green fluorescence (λ_{em} = 555 nm) was restored in PBS buffer (0.5% DMSO, 10 mM, pH 7.4) solution. The emission enhancement at 555 nm displayed a linear response to formaldehyde concentrations in the range of 0 mM to 0.25 mM with a detection limit of 10 μM. Cell imaging experiments revealed that the sensor was cell permeable and proficient for monitoring exogenous or endogenous formaldehyde in HeLa cells with different emission signals.

Chen *et al.*[118] reported a chemodosimetric probe, **35**, which was demonstrated for selective detection of formaldehyde based on the aza-Cope rearrangement reaction (Fig. 18). The probe **35** possessed a homoallyl amino group that acted as a functional trigger moiety for formaldehyde. In the presence of formaldehyde, an imine formation reaction induced the

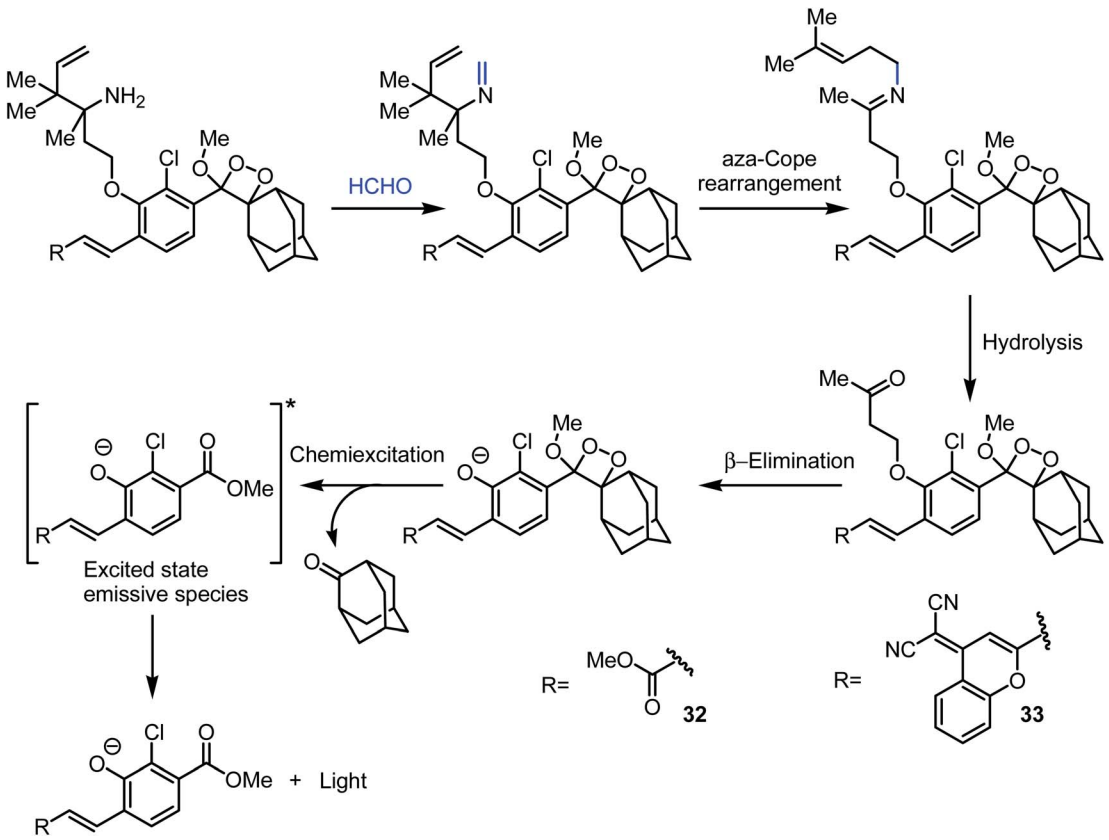

Fig. 16 Reaction of chemodosimeters **32** and **33** with formaldehyde.

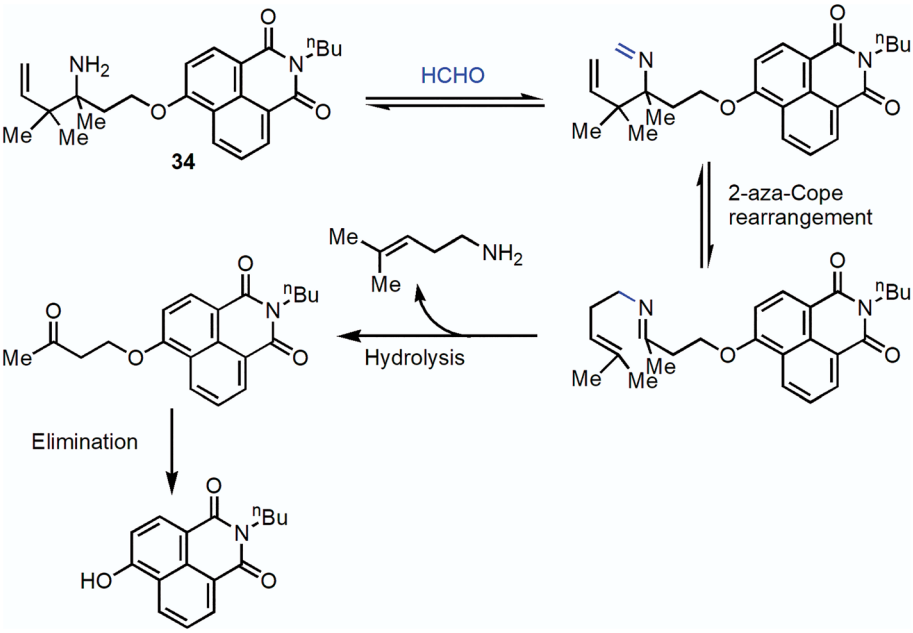

Fig. 17 Reaction of chemodosimeter **34** with formaldehyde.

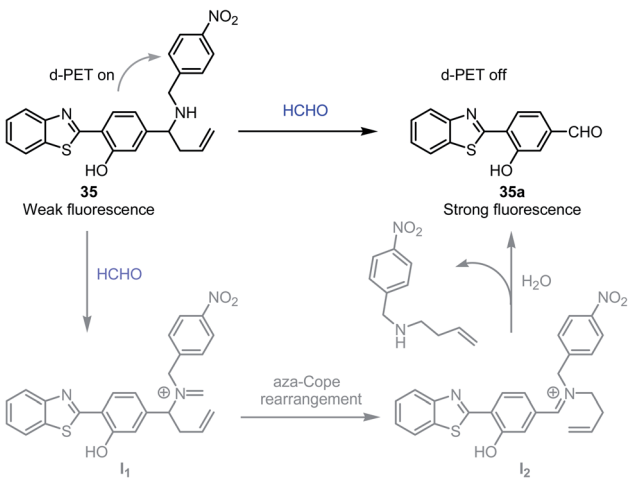

Fig. 18 Reaction of chemodosimeter **35** with formaldehyde.

formation of ($\mathbf{I_1}$), followed by a 2-aza-Cope rearrangement reaction ($\mathbf{I_2}$) and hydrolysis to produce the final product (**35a**). When probe **35** reacted with formaldehyde in PBS buffer–acetonitrile (pH 7.4, 10 mM, 7 : 3, v/v) solution, a gradual increase in fluorescence at 542 nm was observed due to the formation of **35a**. In addition, **35** exhibited good selectivity toward formaldehyde and was unaffected by other potentially competing species (*e.g.* cysteine, GSH, sodium ascorbate, K^+, Na^+, NaClO, H_2O_2, acetone, phenylaldehyde, oxaldehyde, butyraldehyde and formaldehyde). The fluorescence intensity was linearly proportional to the formaldehyde concentration (0–10 mM), and the limit of detection for formaldehyde was calculated to be 2.5×10^{-4} M. Moreover, **35** was able to detect formaldehyde in bovine serum albumin (BSA) samples. Furthermore, test kit experiments revealed that this probe has prospective use for the vapor phase detection of formaldehyde.

Yin and co-workers[119] utilized a perylene-based fluorescent nanoprobe (**36**) to sense formaldehyde in solution as well as in lysosomes. Additionally, red shifts were observed in both the absorption and emission spectra of this sensor in the presence of formaldehyde, with a concomitant emission color change from blue to green. The detection limit of nanoprobe **36** at pH 5 was found to be 0.96 μM. However, this nanoprobe was also utilized for the detection of exogenous and endogenous formaldehyde in live HeLa cells (Fig. 19).

In 2019, Li and co-workers[120] developed an AIE-based ratiometric fluorescent probe (**37**) that acts as a formaldehyde chemodosimeter *via* a formaldehyde promoted aza-Cope reaction. The reaction between probe **37** and formaldehyde yields an aldehyde compound as the only product. This leads to a gradual decrease of the emission intensity at 442 nm with the concurrent appearance of a new red-shifted (46 nm) emission band

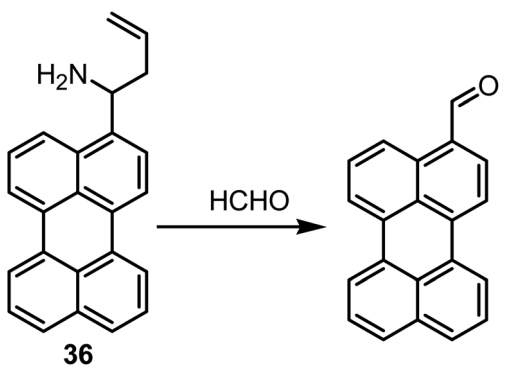

Fig. 19 Reaction of chemodosimeter **36** with formaldehyde.

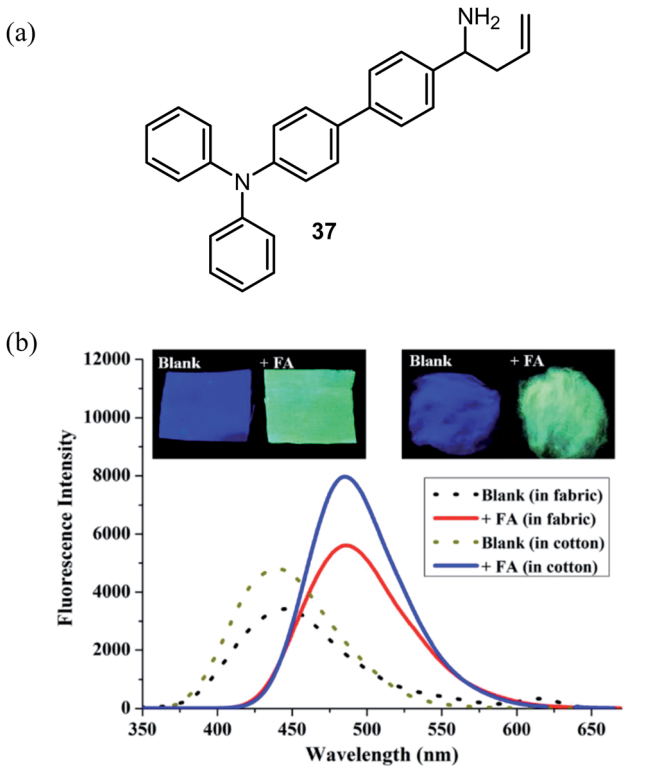

Fig. 20 (a) Reaction of chemodosimeter **37** with formaldehyde. (b) The fluorescence spectra of the fabric and cotton before and after treating with formaldehyde [λ_{ex} = 305 nm]. Inset: photographs of the fabric and cotton taken under a UV lamp (365 nm) before and after treatment with formaldehyde. Reprinted from ref. 120. Copyright (2019), with permission from Elsevier.

centered at 488 nm, which allows the ratiometric sensing of formaldehyde. The experimental solution color changed from deep blue to intense green, which allowed naked eye detection of formaldehyde. The detection limit for formaldehyde was calculated to be 5.1 × 10^{-5} M under the experimental conditions. More importantly, the chemodosimeter **37** was successfully employed for the detection of gaseous formaldehyde in fabric and cotton samples (Fig. 20).

By using a comparable strategy, Liu *et al.*[121] prepared an aggregation-induced emission-based probe (**38**) for the fluorescence turn-on detection of formaldehyde. Because of the photo-induced electron transfer (PET) process, probe **38** showed weak fluorescence in DMSO/H_2O (v/v, 1 : 9) solution. Upon addition of formaldehyde to the solution of **38**, the emission band of the probe at 644 nm demonstrated a noteworthy fluorescence enhancement. The probe **38** could be employed to image formaldehyde in living HeLa cells and mice. The authors developed portable solid test plates for selective, sensitive and quantitative detection of gaseous formaldehyde (Fig. 21). Moreover, this probe was also used for the determination of formaldehyde levels in human serum samples.

Using a similar approach to the above, Lin and co-workers[122] explored a two-photon fluorescent probe **39** based on a coumarin derivative for the detection of formaldehyde in PBS (pH 7.4, 5% DMSO) solution, as well as in living cells and

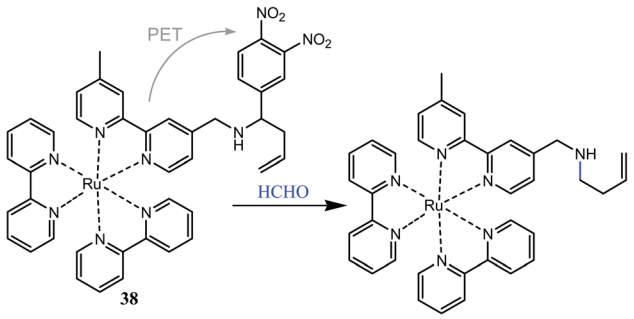

Fig. 21 Reaction of chemodosimeter **38** with formaldehyde.

tissues. Upon addition of formaldehyde, chemodosimeter **39** underwent a 2-aza-Cope sigmatropic rearrangement reaction followed by hydrolysis to yield an aldehyde compound (λ_{ex} = 405 nm, λ_{em} = 451 nm). The emission intensity at 451 nm decreased linearly with the formaldehyde concentration from 0 to 20 μM. The limit of detection of **39** for sensing formaldehyde was estimated to be 4.16 × 10^{-5} M. Two-photon bioimaging of formaldehyde in living cells and tissues with probe **39** was also demonstrated.

Chemodosimeter **40** was synthesized by Hao *et al.*[123] and employed as a ratiometric fluorescent probe for formaldehyde sensing. Upon incremental addition of formaldehyde to the phosphate buffer/DMSO (1 : 1, v/v, pH 7.4, 10 mM) solution of **40**, the emission band at 492 nm decreased gradually, whereas the emission band at 552 nm increased, accompanied with a fluorescence color change from bright cyan to bright yellow. Similarly, in the presence of formaldehyde, the absorption band of probe **40** at 392 nm shifted to a new absorption band at 452 nm, *i.e.*, a red shift of 60 nm, resulting in a color change from colorless to yellowish. These noticeable changes in the optical properties suggested that the aldehyde product was formed by the reaction between formaldehyde and **40**. The authors used HPLC chromatogram analysis to monitor this reaction. The detection limit of formaldehyde was 0.58 μM. Other interfering analytes tested did not cause any considerable changes in the fluorescence of probe **40**. Moreover, the probe was used to image formaldehyde in HeLa cells and in zebrafish. Notably, chemodosimeter **40** was used to monitor formaldehyde concentration in several water samples.

In 2020, Chen *et al.*[124] employed the aza-Cope rearrangement reaction approach for a series of fluorescent probes (**41–45**), which were able to emit emission in a turn-on fashion. All these probes showed high selectivity for formaldehyde over other competitive analytes. Importantly, probe **41** was biocompatible and was employed for imaging formaldehyde in living cells and mouse brains.

The carbazole-based ratiometric fluorescent probe **46** for formaldehyde was designed and synthesized by Gu *et al.*[125] in 2020. Chemodosimeter **46** contains a reactive homoallylamine moiety that serves as a formaldehyde-specific trigger moiety. It was found that the reaction between **46** and formaldehyde resulted in a decrease in the initial strong blue emission band at 393 nm and the formation of a new green emission band

centered at 542 nm. The emission intensity ratio ($I_{542\ nm}/I_{393\ nm}$) displayed a good linear relationship with the formaldehyde concentration in the range of 10–800 μM, and the detection limit was found to be 1.55 μM. In contrast, no apparent emission changes were observed in the presence of benzaldehyde, acetaldehyde, methylglyoxal, H_2O_2, GSH, Cys, Hcy, glucose, sodium ascorbate or NaClO. Here, the sensing mechanism involves the reaction of formaldehyde with the homoallylamine moiety to yield the aldehyde compound *via* a 2-aza-Cope reaction. The sensing mechanism was established by ^{1}H-NMR titration and DFT experiments. Additionally, probe **46** was employed for imaging applications in HeLa cells (Fig. 22).

In 2020, Mengwen *et al.*[126] reported a metal–organic framework (MOF)-based fluorescent probe, **47**, which could selectively and effectively detect formaldehyde based on an aza-Cope rearrangement reaction, as shown in Fig. 23. Probe **47** is non-fluorescent in DMF and Tris buffer solution (7 : 3, v/v). Upon gradual addition of formaldehyde to **47**, the emission intensity at 438 nm increased rapidly and the color of the tested solution changed from colorless to blue. The emission intensity at 438 nm was linearly proportional to the formaldehyde concentration (0 to 25 mM), with a limit of detection of 2.3 μM. The rate constant of the pseudo-first order reaction of **47** with formaldehyde was 7.93 min^{-1}. The authors devised paper strips for detection of formaldehyde gas.

Very recently, Maitra and co-workers[127] developed two pro-sensitizers (**48** and **49**) based on a "turn-on" terbium (Tb^{3+}) photoluminescence strategy for the selective and sensitive detection of formaldehyde. Both probes contained a homoallyl amine moiety as the reactive site for formaldehyde sensing. In the absence of formaldehyde, probes **48** and **49** did not sensitize Tb^{3+}; however, they were able to sensitize Tb^{3+} in terbium cholate (TbCh) hydrogel in the presence of formaldehyde and displayed "turn-on" green fluorescence. The sensing process includes the reaction of formaldehyde with the imine group of the compound to produce the imine intermediate (**X**), which is subjected to a 2-aza-Cope rearrangement reaction to form intermediate **Y**. Upon hydrolysis, the intermediate **Y** was converted to the sensitizer **P**, which sensitized terbium lanthanide in a lanthanide cholate hydrogel matrix, leading to green fluorescence and hence activating the formaldehyde sensing. The authors also reported that these pro-sensitizers could detect formaldehyde not only in solution phase but also in gaseous phase (Fig. 24).

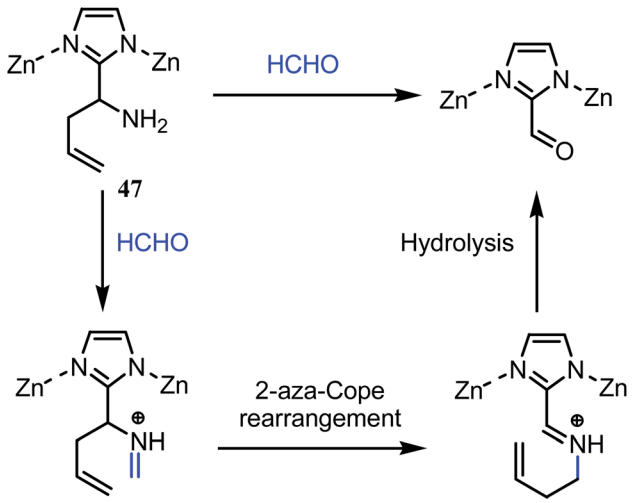

Fig. 23 Reaction of chemodosimeter **47** with formaldehyde.

The aza-Cope reaction showcases the advantages of activity-based detection,[128] first by the formation of a Schiff base with the formaldehyde and then by rearrangement with the assistance of the homoallyl moiety. Importantly, these probes are sustained in multiple environments, including biological systems, which in turn aids their use in physiological systems and in imaging studies. However, the slow reaction kinetics of the reactions hinders their wider applicability. In conventional synthesis, 2-aza-Cope reactions are often performed at elevated temperature in order to achieve first order reaction kinetics. Appropriate structural modification of the homoallyl moiety could overcome this issue; then, the probes could be widely utilized in physiological conditions. Overall improvement of

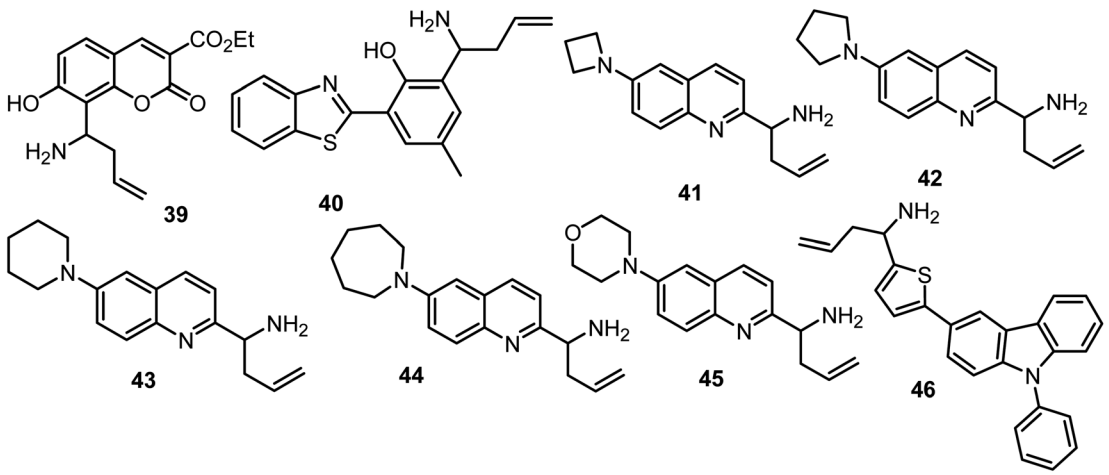

Fig. 22 Structures of formaldehyde probes **39**–**46**.

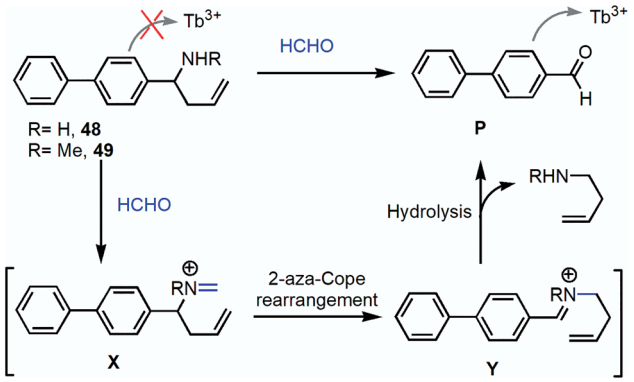

Fig. 24 Reaction of chemodosimeter **48** and **49** with formaldehyde.

this approach is impressive to date; however, further efforts towards this strategy will enable the achievement of the desired goal.

2.3. Miscellaneous approaches

In addition to the abovementioned approaches, several strategies have been devised for the design of formaldehyde sensors. These are relatively new emerging strategies that have been proved to be effective for the detection of formaldehyde. Very few reports exist of these mechanisms; consequently, there is great room for execution and improvement of these strategies.

In 2018, Costero and coworkers[129] reported a phenethylamine-based chemodosimeter (**50**) which showed excellent selectivity for formaldehyde over other different VOCs, including methanol, acetone, toluene, acetaldehyde, benzaldehyde and CO_2. The fluorescence was turned on in the presence of formaldehyde, mainly due to a Pictet–Spengler reaction, as shown in Fig. 25. The detection limit for formaldehyde in solution phase was estimated to be 0.24 mM. The author also developed test strips for colorimetric detection of formaldehyde in contaminated real atmospheres.

Lin and co-workers[130] reported a FRET-based ratiometric fluorescent probe (**51**) for the selective detection of SO_2 and formaldehyde. The probe **51** rapidly interacts with SO_2, resulting in a sulfonylated probe (**51a**) with a blue shift of λ_{ex} (85 nm). Sulfonylated probe **51a** showed excellent sensitivity towards formaldehyde and immediately reverted to the parent probe **51**, accompanied by a red shift in the emission band from 550 nm to 635 nm. This probe was further employed to image formaldehyde in living systems (Fig. 26).

Similarly, carbazole–benzopyrylium-based chemodosimeters **52** and **53** were reported by Lin and co-workers[131] for the selective and sensitive detection of sulfur dioxide and formaldehyde in HEPES buffer solution (10 mM, pH 7.0,

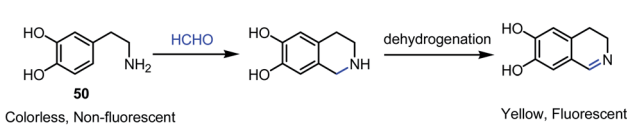

Fig. 25 Reaction of chemodosimeter **50** with formaldehyde.

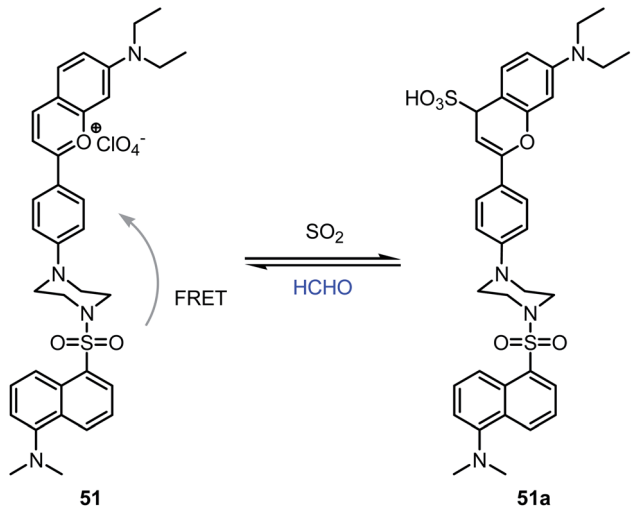

Fig. 26 Reaction of chemodosimeter **51** with formaldehyde.

containing 20% CH_3CN). Upon incremental addition of formaldehyde to probe **52** solution, an increase in the emission intensity at 635 nm was found, followed by a mild decrease at 425 nm. However, probe **53** showed fluorescence peaks that shifted from 370 nm to 630 nm when detecting formaldehyde (Fig. 27). Between these two probes, **53** (recovered time less than 1 min) was more effective for the sensing of formaldehyde than **52** (recovered time 30 min). Cell imaging experiments confirmed that **53** was proficient to monitor exogenous and endogenous formaldehyde in living cells, living zebrafish and murine species.

Squarine-based colorimetric and water soluble fluorescent chemodosimeters **54** and **55** was devised by Fang and co-workers[132] for the detection of various aldehydes, including formaldehyde, acetaldehyde, glyoxal, glutaric dialdehyde, propionaldehyde and pyridine-2-carboxaldehyde, in aqueous medium. The sensing mechanism was based on the nucleophilic attack of the hydrazine to the four-membered rings of squarine to generate hydrazine adduct (**B**) and a further imine formation in the presence of aldehyde (**C** and **D**), followed by

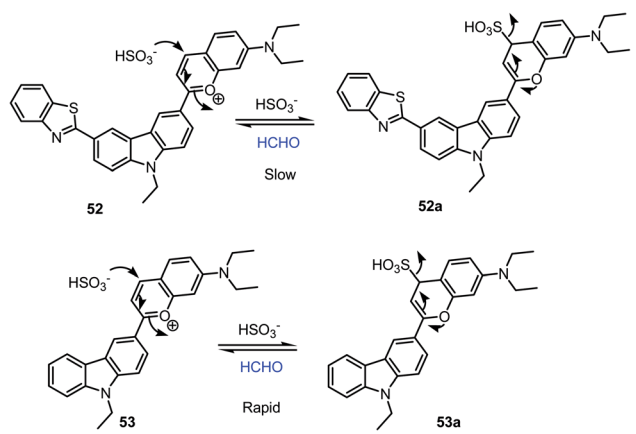

Fig. 27 Reaction of chemodosimeters **52** and **53** with formaldehyde.

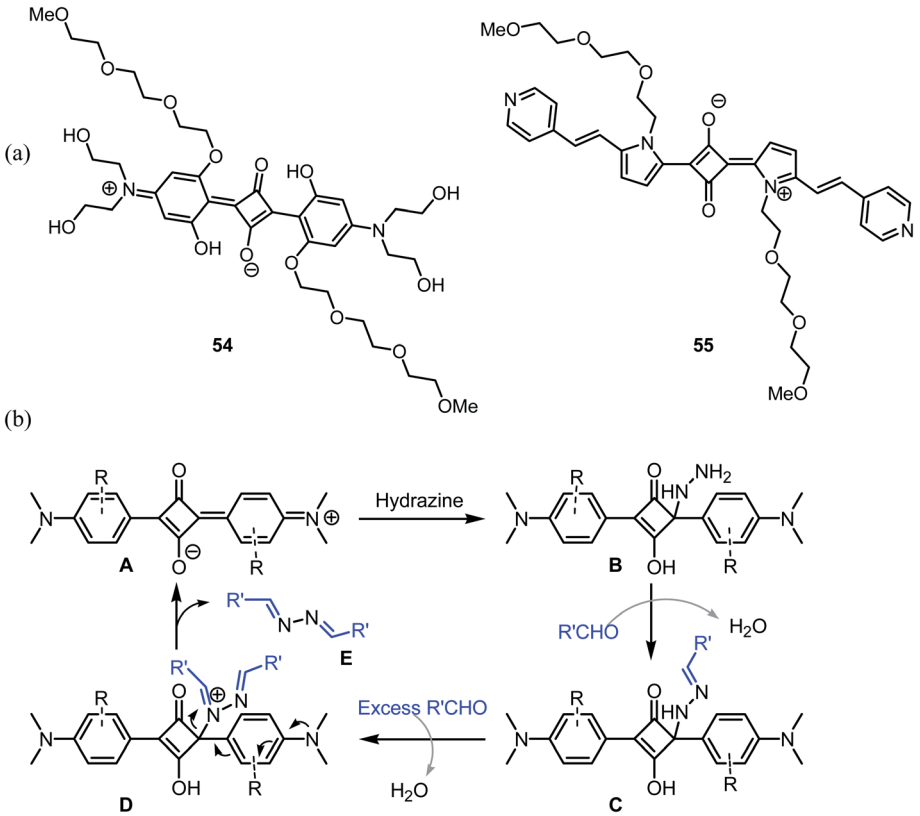

Fig. 28 (a) Structures of chemodosimeters **54** and **55** and (b) reaction mechanism of the chemodosimeters with formaldehyde.

the removal of **E** to regenerate the chemodosimeter (**A**). This sensing mechanism was supported by mass spectroscopy studies. Importantly, the detection limit of **54** for formaldehyde was found to be 60 μM (Fig. 28).

Recently, Wei *et al.*[133] reported a near-infrared (NIR)-based colorimetric probe **56** for the detection of formaldehyde in methanol solution. Probe **56** showed a maximum absorption band at 720 nm; however, when formaldehyde and 5% acetic acid were added, a color change from blue to green was noted as a consequence of the red-shift of the absorption band from 720 nm to 800 nm. The ratio of the absorptions of probe **56** at 800 nm and 720 nm (A_{800}/A_{720}) exhibited a good linear relationship with the formaldehyde concentration between 0 and 1.2 mM, and the detection limit was determined to be 3.25 μM. However, addition of formaldehyde and acetic acid to the probe's solution led to a decrease in the emission band. Probe **56** was also evaluated in the presence of acetone, 1,4-phthalaldehyde, 5-hydroxy-2-nitrobenzaldehyde, 5-bromosalicylaldehyde, 2,4-dichlorobenzaldehyde, and 4-methoxybenzaldehyde; however, no changes in the optical properties were found. The sensing mechanism was mainly based on the imine formation reaction, followed by protonation of the piperazine moiety to form green product **56a**. In addition, probe **56** was employed to detect formaldehyde in both solution and gaseous phases by handy test papers (Fig. 29).

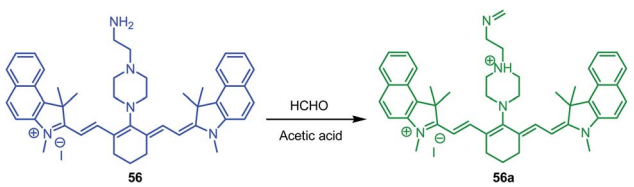

Fig. 29 Reaction of chemodosimeter **56** with formaldehyde.

3. Conclusion and perspective

In this review, we have summarized recent developments in fluorescent probes for the detection of formaldehyde in both living systems and the environment, emphasizing the mechanistic understanding of the various types of fluorometric/colorimetric sensors and their potential application in bioimaging. Importantly, a sharp color change of the solution of several probes upon selective sensing of formaldehyde helps to monitor the process by the naked eye, which eventually inspired researchers to apply this chemistry in real-life applications. A few authors developed solid "test kits" that act as "dip-in" sensors for selective detection of vapor phase formaldehyde. Due to their good cell permeability and low cytotoxic nature, many probes can be used for imaging (*in vitro*/*in vivo*) formaldehyde in biological samples. On the other hand, few probes have also been used for detection of formaldehyde in real food and environment samples. Despite the numerous applications of the developed chemodosimeters for selective detection of formaldehyde in biological samples, wider application has been retarded by their non-NIR-based fluorescent properties. NIR

fluorescence imaging is an expedient and non-invasive imaging technique for visualizing and tracking different biological analytes *in vitro* and *in vivo*, as it possesses meticulous tissue penetration strength with insignificant damage. Therefore, the design and synthesis of NIR-based fluorescent probes is sought to be the major target for the future level of research on this topic. A major impediment of the developed strategies is the necessity of a stoichiometric amount of fluorescent probe to generate a fluorescence signal, resulting in an inefficient and expensive approach. Additionally, it disequilibrates the native analyte homoeostasis and local concentration levels. Thus, it is highly desirable to develop reversible fluorescent probes for recycling of these compounds to prevent the generation of chemical waste. A detailed understanding of the mechanism of the fluorescent probes could help chemists to develop anticipated reversible probes, which will help to curb the limitations of the current chemical tools. We hope that this detailed discussion on the sensing mechanisms and collective summaries of recent developments will be helpful and will encourage the scientific fraternity to become involved in developing new sensing probes for the further design and development of anticipated reversible chromogenic and fluorogenic probes for selective formaldehyde detection.

Conflicts of interest

The authors declare no conflict of interest for this manuscript.

Acknowledgements

SKM would like to thank Mr Shubham Ray and Miss Eti Patra for their valuable assistance in preparing the manuscript. SM thanks UGC, New Delhi, India for the DSK Postdoctoral fellowship (award no. F.4-2/2006(BSR)/CH/17-18/0097).

References

1 H. R. Gerberich and G. C. Seaman, in *Formaldehyde Encyclopedia of Chemical Technology*, Wiley, New York, 4th edn, 1994, vol. 11, pp. 929–951.
2 T. Salthammer, S. Mentese and R. Marutzky, *Chem. Rev.*, 2010, **110**, 2536.
3 R. G. Liteplo and M. E. Meek, *J. Toxicol. Environ. Health, Part B*, 2003, **6**, 85.
4 R. G. Liteplo, R. Beauchamp, M. E. Meek and R. Chénier, *Formaldehyde (Concise International Chemical Assessment Documents)*, World Health Organization, Geneva, 2002.
5 R. J. Scheuplein, *Adv. Chem.*, 1985, **210**, 237.
6 B. A. Kottes Andrews and R. M. Reinhardt, *Adv. Chem.*, 1985, **210**, 83.
7 N. Muttil, G. Ravichandra, S. W. Bigger, G. R. Thorpe, D. Shailaja and S. K. Singh, *Procedia Mater. Sci.*, 2014, **6**, 2.
8 F. Nowshad, M. N. Islam and M. S. Khan, *Agric. Food Secur.*, 2018, **7**, 1.
9 H. E. Jass, *Adv. Chem.*, 1985, **210**, 229.
10 B. Meyer and K. Hermanns, in *Formaldehyde*, American Chemical Society, 1985, ch. 8, vol. 210, pp. 101–116.
11 A. Moghaddam, W. Olszewska, B. Wang, J. S. Tregoning, R. Helson, Q. J. Sattentau and P. J. Openshaw, *Nat. Med.*, 2006, **12**, 905.
12 J. L. Costa and D. L. Murphy, *Nature*, 1975, **255**, 407.
13 X. Tang, Y. Bai, A. Duong, M. T. Smith, L. Li and L. Zhang, *Environ. Int.*, 2009, **35**, 1210.
14 M. A. Flyvholm and P. Andersen, *Am. J. Ind. Med.*, 1993, **24**, 533.
15 J. R. Beall and A. G. Ulsamer, *J. Toxicol. Environ. Health*, 1984, **14**, 1.
16 C. Martínez-Aquino, A. M. Costero, S. Gil and P. Gaviña, *Nanomaterials*, 2019, **9**, 302.
17 V. J. Cogliano, Y. Grosse, R. A. Baan, K. Straif, M. B. Secretan and F. E. Ghissassi, *Environ. Health Perspect.*, 2005, **113**, 1205.
18 R. G. Liteplo, R. Beauchamp, M. E. Meek and R. Chenier, *Formaldehyde (Concise International Chemical Assessment Documents)*, World Health Organization, Geneva, 2002.
19 R. Baan, Y. Grosse, K. Straif, B. Secretan, F. El Ghissassi, V. Bouvard, L. Benbrahim-Tallaa, N. Guha, C. Freeman, L. Galichet and V. Cogliano, *Lancet Oncol.*, 2009, **10**, 1143.
20 *Formaldehyde Analytical Chemistry and Toxicology*, ed. V. Turoski, ACS Advances in Chemistry Series 210, American Chemical Society, Washington, DC, 1985.
21 P. Patnaik, *Handbook of Environmental Analysis. Chemical Pollutants in Air, Water, Soil, and Solid Wastes*, CRC Press, Boca Raton, FL, 1997.
22 R. C. Chautems, X. Delgadillo, L. Rubbia-Brandt, J. P. Deleaval, M.-C. L. Marti and B. Roche, *Colorectal Dis.*, 2003, **5**, 24.
23 N. Gaudin and Y. Grosse, *IARC classifies formaldehyde as carcinogenic to humans*, International Agency for Research on Cancer, Press Release, No 153, Jun, 2004.
24 K. C. Gupta, A. G. Ulsamer and P. W. Preuss, *Environ. Int.*, 1982, **8**, 349.
25 Z. He, Y. Zhang and W. Wei, *Build. Environ.*, 2012, **47**, 197.
26 K. Kawamura, K. Kerman, M. Fujihara, N. Nagatani, T. Hashiba and E. Tamiya, *Sens. Actuators, B*, 2005, **105**, 495.
27 B. Meyer and K. Hermanns, *Adv. Chem.*, 1985, **210**, 101.
28 T. Salthammer, S. Mentese and R. Marutzky, Formaldehyde in the indoor environment, *Chem. Rev.*, 2010, **110**, 2536.
29 S. M. Kooistra and K. Helin, *Nat. Rev. Mol. Cell Biol.*, 2012, **13**, 297.
30 Y. Shi, F. Lan, C. Matson, P. Mulligan, J. R. Whetstine, P. A. Cole, R. A. Casero and Y. Shi, *Cell*, 2004, **119**, 941.
31 J. O'Sullivan, *Neurotoxicology*, 2004, **25**, 303.
32 J. R. Whetstine, A. Nottke, F. Lan, M. Huarte, S. Smolikov, Z. Chen, E. Spooner, E. Li, G. Zhang and M. Colaiacovo, *Cell*, 2006, **125**, 467.
33 P. A. Cloos, J. Christensen, K. Agger, A. Maiolica, J. Rappsilber, T. Antal, K. H. Hansen and K. Helin, *Nature*, 2006, **442**, 307.
34 J. R. Whetstine, A. Nottke, F. Lan, M. Huarte, S. Smolikov, Z. Chen, E. Spooner, E. Li, G. Zhang, M. Colaiacovo and Y. Shi, *Cell*, 2006, **125**, 467.

35 R. J. Klose, K. Yamane, Y. Bae, D. Zhang, H. Erdjument-Bromage, P. Tempst, J. Wong and Y. Zhang, *Nature*, 2006, **442**, 312.
36 H. d. A. Heck, M. Casanova-SchmTz, P. B. Dodd, E. N. Schachter, T. J. Witek and T. Tosun, *Am. Ind. Hyg. Assoc. J.*, 1985, **46**, 1.
37 Z. Tong, C. Han, W. Luo, X. Wang, H. Li, H. Luo, J. Zhou, J. Qi and R. He, *Age*, 2013, **35**, 583.
38 A. Songur, O. A. Ozen and M. Sarsilmaz, *Rev. Environ. Contam. Toxicol.*, 2010, **203**, 105.
39 Z. Tong, C. Han, W. Luo, H. Li, H. Luo, M. Qiang, T. Su, B. Wu, Y. Liu, X. Yang, Y. Wan, D. Cui and R. He, *Sci. Rep.*, 2013, **3**, 1807.
40 C. M. Thompson, R. Ceder and R. C. Grafström, *Toxicol. Lett.*, 2010, **193**, 1.
41 J. Miao and R. He, *Chronic Formaldehyde-mediated impairments and age-related dementia*, InTech, Shanghai, 2012, pp. 59–77.
42 C. Bosetti, J. K. McLaughlin, R. E. Tarone, E. Pira and C. L. Vecchia, *Ann. Oncol.*, 2008, **19**, 29.
43 J. D. Thrasher and K. H. Kilburn, *Arch. Environ. Health*, 2001, **56**, 300.
44 G. P. Voulgaridou, I. Anestopoulos, R. Franco, M. I. Panayiotidis and A. Pappa, *Mutat. Res.*, 2011, **711**, 13.
45 L. Zhang, C. Steinmaus, D. A. Eastmond, X. K. Xin and M. T. Smith, *Mutat. Res.*, 2009, **981**, 150.
46 A. Lino-dos-Santos-Franco, H. V. Domingos, A. P. L. De Oliveira, A. C. Breithaupt-Faloppa, J. P. S. Peron, S. Bolonheis, M. N. Muscará, R. M. Oliveira-Filho, B. B. Vargaftig and W. Tavares-de-Lima, *Toxicol. Lett.*, 2010, **197**, 211.
47 K. Tulpule and R. Dringen, *J. Neurochem.*, 2013, **127**, 7.
48 P. A. Jones, *Nat. Rev. Genet.*, 2012, **13**, 484.
49 I. Broder, P. Corey, P. Brasher, M. Lipa and P. Cole, *Environ. Health Perspect.*, 1991, **95**, 101.
50 M. Hauptmann, P. A. Stewart, J. H. Lubin, L. E. Beane Freeman, R. W. Hornung, R. F. Herrick, R. N. Hoover, J. F. Fraumeni Jr, A. Blair and R. B. Hayes, *J. Natl. Cancer Inst.*, 2009, **101**, 1696.
51 Z. Tong, J. Zhang, W. Luo, W. Wang, F. Li, H. Li, H. Luo, J. Lu, J. Zhou, Y. Wan and R. He, *Neurobiol. Aging*, 2011, **32**, 31.
52 M. Unzeta, M. Sole, M. Boada and M. Hernandez, *J. Neural Transm.*, 2007, **114**, 857.
53 H. Reingruber and L. B. Pontel, *Curr. Opin. Toxicol.*, 2018, **9**, 28.
54 *WHO Guidelines for Indoor Air Quality: Selected Pollutants*, WHO Regional Office for Europe, Copenhagen, 2010.
55 *Formaldehyde (CASRN 50-00-0). Integrated Risk Information System. Document 0419*, U.S. Environmental Protection Agency, Washington, D.C., 1998.
56 S. E. Sayed, L. Pascual, M. Licchelli, R. Martínez-Máñez, S. Gil, A. M. Costero and F. Sancenón, *ACS Appl. Mater. Interfaces*, 2016, **8**, 14318.
57 World Health Organisation, *Guidelines for Drinking-Water Quality*, Geneva, 2nd edn, 1993, vol. 2, health criteria and other supporting information.
58 P. H. Yu and C. Cauglin, *Anal. Biochem.*, 2003, **318**, 285.
59 P. Yang and C. W. Lau, *Luminescence*, 2007, **22**, 473.
60 H. Ohata and M. Otsuka, *J. Chromatogr. B: Biomed. Sci. Appl.*, 1997, **693**, 297.
61 D. Shi and L. Wei, *Sens. Actuators, B*, 2013, **177**, 370.
62 T. Itoh and I. Matsubara, *Sens. Actuators, B*, 2008, **128**, 512.
63 K. Mitsubayashi and H. Matsunga, *Sens. Actuators, B*, 2005, **108**, 660.
64 S. Dong and P. K. Dasgupta, *Environ. Sci. Technol.*, 1986, **20**, 637.
65 M. Lofdahl and C. Utaiwasin, *Sens. Actuators, B*, 2001, **80**, 183.
66 J. M. Lorrain, C. R. Fortune and B. Dellinger, *Anal. Chem.*, 1981, **53**, 1302.
67 J. C. Septon and J. C. Ku, *Am. Ind. Hyg. Assoc. J.*, 1982, **43**, 845.
68 Z. Zhang, C. Zhao, Y. Ma and G. Li, *Analyst*, 2014, **139**, 3614.
69 O. Bunkoed, F. Davisc, P. Kanatharana, P. Thavarungkul and S. P. J. Higson, *Anal. Chim. Acta*, 2010, **659**, 251.
70 Y. Zhu and H. Li, *Langmuir*, 2012, **28**, 7843.
71 M. J. Dennison, J. M. Hall and A. P. F. Turner, *Analyst*, 1996, **121**, 1769.
72 F. C. Chung, R. J. Wu and F. C. Cheng, *Sens. Actuators, B*, 2014, **190**, 1.
73 A. Bi, S. Yang, M. Liu, X. Wang, W. Liao and W. Zeng, *RSC Adv.*, 2017, **7**, 36421.
74 X. Liu, N. Li, M. Li, H. Chen, N. Zhang, Y. Wang and K. Zheng, *Coord. Chem. Rev.*, 2020, **404**, 213109.
75 Z. Xu, J. Chen, L.-L. Hu, Y. Tan, S.-H. Liu and J. Yin, *Chin. Chem. Lett.*, 2017, **28**, 1935.
76 Y. Tang, Y. Ma, J. Yin and W. Lin, *Chem. Soc. Rev.*, 2019, **48**, 4036.
77 K. J. Bruemmer, T. F. Brewer and C. J. Chang, *Curr. Opin. Chem. Biol.*, 2017, **39**, 17.
78 N. Kwon, D. Kim, K. M. K. Swamy and J. Yoon, *Coord. Chem. Rev.*, 2021, **427**, 213581.
79 A. C. Sedgwick, L. Wu, H.-H. Han, S. D. Bull, X.-P. He, T. D. James, J. L. Sessler, B. Z. Tang, H. Tian and J. Yoon, *Chem. Soc. Rev.*, 2018, **47**, 8842.
80 D. Banik, S. K. Manna and A. K. Mahapatra, *Spectrochim. Acta, Part A*, 2021, **246**, 119047.
81 X. Zhou, S. Lee, Z. Xu and J. Yoon, *Chem. Rev.*, 2015, **115**, 7944.
82 S. K. Manna, A. Gangopadhyay, K. Maiti, S. Mondal and A. K. Mahapatra, *ChemistrySelect*, 2019, **4**, 7219.
83 H. Schiff, *Justus Liebigs Ann. Chem.*, 1864, **131**, 118.
84 U. Schiff, *Giornale di scienze naturali ed economiche*, 1866, **2**, 201.
85 L. Fabbrizzi, *J. Org. Chem.*, 2020, **85**, 12212.
86 H. Song, S. Rajendiran, N. Kim, S. K. Jeong, E. Koo, G. Park, T. D. Thangadurai and S. Yoon, *Tetrahedron Lett.*, 2012, **53**, 4913.
87 Y. Wu, Z. Zheng, J. Wen, H. Li, S. Sun and Y. Xu, *Sens. Actuators, B*, 2018, **260**, 937.
88 T. Cao, D. Gong, S.-C. Han, A. Iqbal, J. Qian, W. Liu, W. Qin and H. Guo, *Talanta*, 2018, **189**, 274.

89 A. Gangopadhyay, K. Maiti, S. S. Ali, A. K. Pramanik, U. N. Guria, S. K. Samanta, R. Sarkar, P. Datta and A. K. Mahapatra, *Anal. Methods*, 2018, **10**, 2888.
90 W. Chen, J. Han, X. Wang, X. Liu, F. Liu, F. Wang, R.-Q. Yu and J.-H. Jiang, *ACS Omega*, 2018, **3**, 14417.
91 N. Hidayah, B. Purwono, B. A. Nurohmah and H. D. Pranowo, *Indones. J. Chem.*, 2019, **19**, 1074.
92 H.-R. Cheng, L.-W. Zou, L. Yang, Z.-G. Wang and X.-J. Lu, *ChemistrySelect*, 2019, **4**, 432.
93 W. Chen, M. Yang, N. Luo, F. Wang, R.-Q. Yu and J.-H. Jiang, *Analyst*, 2019, **144**, 6922.
94 K. Wechakorn, S. Supalang and S. Suanpai, *Tetrahedron*, 2020, **76**, 131411.
95 H. Ding, G. Yuan, L. Peng, L. Zhou and Q. Lin, *J. Agric. Food Chem.*, 2020, **68**, 3670.
96 C. Liu, C. Shi, H. Li, W. Du, Z. Li, L. Wei and M. Yu, *Sens. Actuators, B*, 2015, **219**, 185.
97 S. Nandi, E. Sharma, V. Trivedi and S. Biswas, *Inorg. Chem.*, 2018, **57**, 15149.
98 A. Xu, Y. Tang and W. Lin, *New J. Chem.*, 2018, **42**, 8325.
99 P. Li, D. Zhang, Y. Zhang, W. Lu, W. Wang and T. Chen, *ACS Sens.*, 2018, **3**, 2394.
100 H.-W. Chen, H. Li and Q.-H. Song, *ACS Omega*, 2018, **3**, 18189.
101 F. Xin, Y. Tian, C. Gao, B. Guo, Y. Wu, J. Zhao, J. Jing and X. Zhang, *Analyst*, 2019, **144**, 2297.
102 F. Xin, Y. Tian, J. Jing and X. Zhang, *Anal. Methods*, 2019, **11**, 2969.
103 Y. Cao, Z. Teng, J. Zhang, T. Cao, J. Qian, J. Wang, W. Qin and H. Guo, *Sens. Actuators, B*, 2020, **320**, 128354.
104 G. Hongwei, L. Guoqiang, Y. Ranhao, S. Zhenli, C. Hongxia, Y. Long, S. Pengchen, S. Mingtai, K. A. Alamry, H. M. Marwani and W. Suhua, *Microchem. J.*, 2020, **156**, 104793.
105 W. Yuan, X. Zhong, Q. Han, Y. Jiang, J. Shen and B. Wang, *J. Photochem. Photobiol., A*, 2020, **400**, 112701.
106 L. Jiang, Q. Hu, T. Chen, D. Min, H.-Q. Yuan and G.-M. Bao, *Spectrochim. Acta, Part A*, 2020, **228**, 117789.
107 A. L. Berhanu, Gaurav, I. Mohiuddin, A. K. Malik, J. S. Aulakh, V. Kumar and K.-H. Kim, *TrAC, Trends Anal. Chem.*, 2019, **116**, 74.
108 L. E. Overman, P. G. Humphreys and G. S. Welmaker, *Org. React.*, 2011, **75**, 747.
109 A. Roth, H. Li, C. Anorma and J. Chan, *J. Am. Chem. Soc.*, 2015, **137**, 10890.
110 X. Yang, L. He, K. Xu, Y. Yang and W. Lin, *Anal. Methods*, 2018, **10**, 2963.
111 X. Zhao, C. Ji, L. Ma, Z. Wu, W. Cheng and M. Yin, *ACS Sens.*, 2018, **3**, 2112.
112 D. Zhang, D. Liu, M. Li, Y. Yang, Y. Wang, H. Yin, J. Liu, B. Jia and X. Wu, *Anal. Chim. Acta*, 2018, **1033**, 180.
113 M. Yang, J. Fan, J. Du, S. Long, J. Wang and X. Peng, *Front. Chem.*, 2018, **6**, 488.
114 X. Yang, L. He, K. Xu, Y. Yang and W. Lin, *New J. Chem.*, 2018, **42**, 12361.
115 H. Yang, G. Fang, M. Guo, P. Ning, Y. Feng, H. Yu and X. Meng, *Sens. Actuators, B*, 2018, **270**, 318.
116 K. J. Bruemmer, O. Green, T. A. Su, D. Shabat and C. J. Chang, *Angew. Chem., Int. Ed.*, 2018, **57**, 7508.
117 Z. Xie, B. Yin, J. Shen, D. Hong, L. Zhu, J. Ge and Q. Zhu, *Org. Biomol. Chem.*, 2018, **16**, 4628.
118 H. Chen, Y. Zhou, K. Zheng, N. Zhang, X. Tan and W. Chen, *ChemistrySelect*, 2019, **4**, 9622.
119 C. Ji, L. Ma, H. Chen, Y. Cai, X. Zhao and M. Yin, *ACS Appl. Bio Mater.*, 2019, **2**, 555.
120 B. Zhai, Y. Zhang, Z. Hu, J. He, J. Liu, C. Gao and W. Li, *Dyes Pigm.*, 2019, **171**, 107743.
121 C. Liu, R. Zhang, W. Zhang, J. Liu, Y.-L. Wang, Z. Du, B. Song, Z. P. Xu and J. Yuan, *J. Am. Chem. Soc.*, 2019, **141**, 8462.
122 M. Li, X. Kong, B. Dong, N. Zhang, W. Song, Y. Lu and W. Lin, *New J. Chem.*, 2019, **43**, 11844.
123 Y. Hao, Y. Zhang, A. Zhang, Q. Sun, J. Zhu, P. Qu, S. Chen and M. Xu, *Spectrochim. Acta, Part A*, 2020, **229**, 117988.
124 J. Chen, C. Shao, X. Wang, J. Gu, H.-L. Zhu and Y. Qian, *Chem. Commun.*, 2020, **56**, 3871.
125 J. Gu, X. Li, G. Zhou, W. Liu, J. Gao and Q. Wang, *J. Hazard. Mater.*, 2020, **386**, 121883.
126 L. Mengwen, S. Ao, L. Yueqi, Z. Hao, H. Xiaohui, L. Xueliang, S. Xinchao and Y. Yunxu, *Anal. Methods*, 2020, **12**, 3748.
127 D. Bhowmik, A. Dutta and U. Maitra, *Chem. Commun.*, 2020, **56**, 12061.
128 J. Ohata, K. J. Bruemmer and C. J. Chang, *Acc. Chem. Res.*, 2019, **52**, 2841.
129 C. Martínez-Aquino, A. M. Costero, S. Gil and P. Gaviña, *Molecules*, 2018, **23**, 2646.
130 Y. Ma, W. Gao, L. Zhu, Y. Zhao and W. Lin, *Analyst*, 2020, **145**, 1865.
131 Y. Ma, Y. Tang, Y. Zhao and W. Lin, *Anal. Chem.*, 2019, **91**, 10723.
132 T. Liu, L. Yang, J. Zhang, K. Liu, L. Ding, H. Peng, K. D. Belfield and Y. Fang, *Sens. Actuators, B*, 2019, **292**, 88.
133 K. Wei, L. Ma, G. Ma, C. Ji and M. Yin, *Dyes Pigm.*, 2019, **165**, 294.